URATv1であり，管腔側のURAT1とタンデムに働くことによって尿酸の経細胞輸送を担うというモデルを提唱した[8]．近年，Genome Wide Association Study（GWAS）によって，血中尿酸値や痛風と関連する遺伝子の報告が多数なされているが，尿酸値は管腔側のURAT1よりも血管側のURATv1の方が遺伝子多型との関連を示されている場合が圧倒的に多い[15-18]．このことと今回の結果を考え合わせると，高尿酸血症発症には管腔側での尿酸の細胞内への取り込みよりも，血管側での尿酸の排出の方がより重要である可能性が示唆される．

以上より，腎近位尿細管管腔側の尿酸再吸収トランスポーターURAT1を過剰発現させても，他の尿酸トランスポーターや尿酸代謝酵素のmRNA発現に変化を及ぼさず，血中・尿中尿酸値も変化しないことが示された．

謝　辞

Tgマウスの作出，ならびに研究遂行に際して御助言をいただいた大阪大学大学院医学系研究科生体システム薬理学，金井好克教授に感謝いたします．Tgマウスの維持，スクリーニング，サンプル調製に協力を頂いた，杏林大学医学部薬理学教室，高橋美知氏に感謝いたします．本研究は科学研究費補助金（特定領域研究，若手研究），財団法人痛風研究会の支援によって一部行われました．

文　献

1）Wu XW, Lee CC, Muzny DM et al：Urate oxidase：primary structure and evolutionary implications. Proc Natl Acad Sci U S A. 86：9412-9416, 1989.
2）中村　徹：高尿酸血症の原因（尿酸排泄低下），高尿酸血症・痛風．新しい診断と治療のABC37，鎌谷直之編，pp34-47，最新医学社，東京，2006.
3）Hediger MA, Johnson RJ, Miyazaki H et al：Molecular physiology of urate transport. Physiology（Bethesda）20：125-133, 2005.
4）E nomoto A, Kimura H, Chairoungdua A：Molecular identification of a renal urate anion exchanger that regulates blood urate levels. Nature 23：447-452, 2002.
5）Ichida K, Hosoyamada M, Hisatome I et al：Clinical and molecular analysis of patients with renal hypouricemia in Japan-influence of URAT1 gene on urinary urate excretion. J Am Soc Nephrol 15：164-173, 2004.
6）Roch-Ramel F, Guisan B, Schild L：Indirect coupling of urate and p-aminohippurate transport to sodium in human brush-border membrane vesicles. Am J Physiol 270：F61-68, 1996.
7）安西尚彦，Jutabha Promsuk，木村徹 他：腎臓の尿酸トランスポーター：最近の進歩 痛風と核酸代謝 33：7-15，2009.
8）Anzai N, Ichida K, Jutabha P et al：Plasma urate level is directly regulated by a voltage-driven urate efflux transporter URATv1（SLC2A9）in humans. J Biol Chem 283：26834-26838, 2008.
9）Matsuo H, Takada T, Ichida K et al：Common defects of ABCG2, a high-capacity urate exporter, cause gout：a function-based genetic analysis in a Japanese population. Sci Transl Med 1:p 5ra11, 2009.
10）Takahashi R, Ueda M：Generation of transgenic rats using YAC and BAC DNA constructs. Methods Mol Biol 597：93-108, 2010.
11）Livak KJ, Schmittgen TD：Analysis of relative gene expression data using real-time quantitative PCR and the 2（-Delta Delta C（T））Method. Methods 25：402-408, 2001.
12）Wu X, Wakamiya M, Vaishnav S et al：Hyperuricemia and urate nephropathy in urate oxidase-deficient mice. Proc Natl Acad Sci U S A 91：742-746, 1994.
13）Eraly SA, Vallon V, Rieg T et al：Multiple organic anion transporters contribute to net renal excretion of uric acid. Physiol Genomics 33：180-192, 2008.

14) Anzai N, Miyazaki H, Noshiro R et al : The multivalent PDZ domain-containing protein PDZK1 regulates transport activity of renal urate-anion exchanger URAT1 via its C terminus. J Biol Chem 279 : 45942-45950, 2004.
15) Döing A, Gieger C, Mehta D et al : SLC2A9 influences uric acid concentrations with pronounced sex-specific effects. Nat Genet 40 : 430-436, 2008.
16) Vitart V, Rudan I, Hayward C et al : SLC2A9 is a newly identified urate transporter influencing serum urate concentration, urate excretion and gout. Nat Genet 40 : 437-442, 2008.
17) Stark K, Reinhard W, Neureuther K et al : Association of common polymorphisms in GLUT9 gene with gout but not with coronary artery disease in a large case-control study. PLoS One 3 : e1948, 2008.
18) Dehghan A, Kötgen A, Yang Q et al : Association of three genetic loci with uric acid concentration and risk of gout : a genome-wide association study. Lancet 372 : 1953-1961, 2008.

J Pharmacol Sci 114, 115 – 118 (2010)

Journal of Pharmacological Sciences
©2010 The Japanese Pharmacological Society

Short Communication

Concentration-Dependent Inhibitory Effect of Irbesartan on Renal Uric Acid Transporters

Makiko Nakamura[1], Naohiko Anzai[2], Promsuk Jutabha[2], Hiroyuki Sato[1], Hiroyuki Sakurai[2], and Kimiyoshi Ichida[1,*]

[1]*Department of Pathophysiology, Tokyo University of Pharmacy and Life Sciences, Tokyo 192-0392, Japan*
[2]*Department of Pharmacology and Toxicology, Kyorin University School of Medicine, Tokyo 181-8611, Japan*

Received March 3, 2010; Accepted July 14, 2010

Abstract. Hyperuricemia is currently recognized as a risk factor for cardiovascular diseases. It has been reported that the angiotensin II–receptor blocker (ARB) losartan decreases serum uric acid level. In this study, the effects of another ARB, irbesartan, on [^{14}C]uric acid–transport activity of renal uric acid reabsorptive transporters URAT1 and URATv1 were examined with *Xenopus* oocytes expressing each transporter. The results showed that irbesartan (100 – 500 μM) inhibited the uptake of uric acid via both transporters. The inhibitory effects of irbesartan exceeded those of losartan and other ARBs, and the results suggest that irbesartan can reduce serum uric acid level.

Keywords: angiotensin II–receptor blocker, transporter, uric acid

Hyperuricemia has been associated with hypertension. Approximately 25% of patients with hypertension have hyperuricemia (1), and approximately 30% of patients with hyperuricemia or gout have hypertension (2). Therefore the effects of antihypertensive drugs on serum uric acid (SUA) level, especially angiotensin II–receptor blockers (ARBs), have been scrutinized in recent years. Losartan has been shown to increase urinary uric acid (UA) excretion and decrease SUA level (3). In contrast, other ARBs such as candesartan and valsartan do not have uricosuric activity (4, 5). Thus, it seems that the ability of each ARB to decrease SUA cannot be predicted until the uricosuric activities of all ARBs are examined. In the present study, we focused on another widely-used ARB, irbesartan. One report showed a tendency for irbesartan to decrease SUA level in hypertensive patients with hyperuricemia (6). Therefore we examined the effect of irbesartan on UA transporters involved in regulating SUA level. The UA transporter URAT1 is involved in lumen-to-cytosol reabsorption of UA along the proximal tubule (7). A sugar transport facilitator family member protein GLUT9 (URATv1) functions as an efflux transporter of UA from tubular cells (8) at the basolateral membrane. Mutation of URAT1 or URATv1 is associated with idiopathic renal hypouricemia (7, 9), indicating URAT1 and URATv1 play a dominant role in UA reabsorption and controlling SUA levels. We used *Xenopus* oocytes expressing URAT1 or URATv1 to examine the *cis*-inhibitory effects of irbesartan at various concentrations.

Cloned human URAT1 and URATv1 were expressed in *Xenopus* oocytes as described previously (7, 8). In brief, defolliculated oocytes were injected with 50 ng of cRNA that was transcribed in vitro using T7 RNA polymerase in the presence of cap analog. After incubation of oocytes in Barth's buffer at 18°C for 2 – 3 days, uptake studies were performed in ND 96 buffer (96 mM NaCl, 2 mM KCl, 1.8 mM $CaCl_2$, 1 mM $MgCl_2$, 5 mM HEPES, pH 7.4) containing 20 μM [^{14}C]UA and ARBs at the indicated concentrations; after 1 h incubation, oocytes were lysed and dried at room temperature. Then the amount of the [^{14}C]UA uptake was measured in a scintillation counter and the uptake rate was determined. For determination of the kinetic parameters, the concentrations of urate were varied from 10 to 1500 μM. Kinetic parameters were obtained by using the Eadie-Hofstee equation. The experiments were performed using 8 – 10 oocytes per experiment and repeated three times. All the data are given as the mean ± S.E.M. Student's *t*-test was used to determine significant differences. A value of $P < 0.05$ was considered to be significant.

Figure 1 illustrates the chemical structures of ARBs

*Corresponding author. ichida@toyaku.ac.jp
Published online in J-STAGE on August 21, 2010 (in advance)
doi: 10.1254/jphs.10064SC

examined in this study. In addition to irbesartan, we tested losartan, telmisartan, candesartan, and valsartan. Figure 2A shows that at concentrations of 300 – 500 μM, all ARBs except candesartan significantly inhibited URAT1-mediated [^{14}C]UA uptake. In the present study, valsartan (500 μM) decreased UA uptake via URAT1. Since the administration of a standard dose of valsartan (2 mg/kg) results in a mean plasma concentration of less than 20 μM (10), it seemed unlikely that, clinically, it had any effect on SUA level. Figure 2A also indicates that irbesartan is more inhibitory than losartan. Figure 2B shows the dependence of inhibition on irbesartan concentration. The percentage of UA uptake relative to the control (no inhibitor) level decreased dose-dependently from 30 to 500 μM, indicating the *cis*-inhibitory effect of irbesartan on the UA uptake via URAT1. Kinetic data (Fig. 2: C and D) showed that the inhibition of irbesartan was non-competitive against URAT1 since irbesartan decreased V_{max} from 21.54 to 9.84 pmol·oocyte^{-1}·h^{-1}, but did not change the K_m (218.08 to 191.45 μM).

The uptake of URATv1-expressing oocytes is shown in Fig. 3. Both irbesartan and telmisartan inhibited URATv1-mediated UA uptake to a similar extent. The concentration dependence (in the range 30 – 500 μM) of irbesartan-mediated inhibition (Fig. 3B) confirmed its ability to block UA uptake by URATv1. The results shown in Fig. 3, C and D demonstrate that irbesartan effected an increase in the the K_m value (325.1 to 721.43 μM) and a decrease in the V_{max} (357.66 to 202.52 pmol·oocyte^{-1}·h^{-1}). Those kinetic parameters indicated that irbesartan inhibited URATv1 in both a competitive manner and a non-competitive manner (mixed inhibition).

The present study has demonstrated, for the first time, that irbesartan inhibits renal UA transporters in vitro. Two UA transporters, URAT1 and URATv1 involved in the transport of UA at the apical and basolateral membrane, respectively, were examined (7, 8), and the inhibitory effects of several ARBs were compared with that of irbesartan. As shown in Fig. 1, ARBs with a single anionic group were the most effective UA transporter inhibitors; losartan, irbesartan, and telmisartan with one anionic group but not candesartan and valsartan with two anionic groups markedly decreased UA-uptake. Although further examination is needed, the blocking ability of irbesartan on UA transporters provides important information about the substrate specificity of UA transporters.

Moreover, the inhibitory effect of irbesartan exceeded that of losartan. A losartan concentration of 500 μM seemed to be too small to inhibit URATv1 (Fig. 3A), which is in accordance with previous reports (1 mM) (8). In contrast, irbesartan significantly decreased the UA-uptake by URAT1 and URATv1 at concentrations of 100 – 500 and 300 – 500 μM, respectively (Figs. 2B and 3B). Since the clinically achievable mean plasma concentrations of losartan and irbesartan are 3 and 6 μM (11, 12), respectively, neither drug can have any effect on SUA level from the basolateral (blood) side of the renal proximal tubules. Nevertheless, the urinary concentration

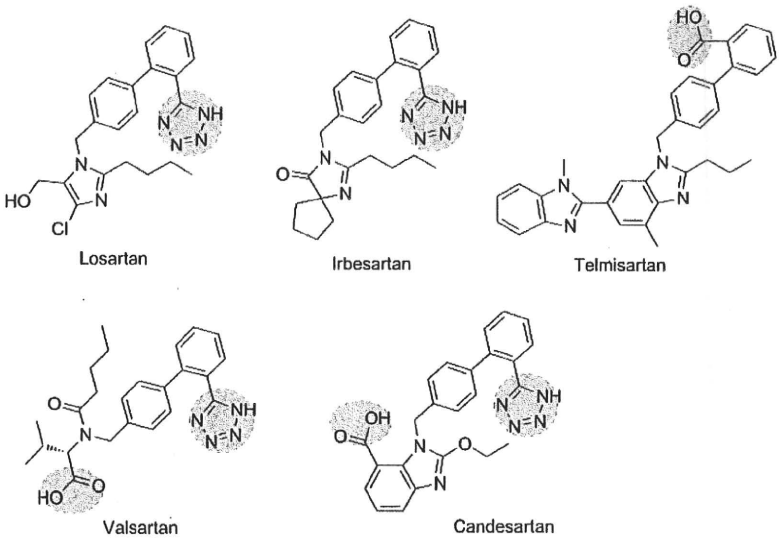

Fig. 1. Chemical structures of angiotensin-receptor blockers (ARBs). Dotted grey circles indicate anionic groups as described in the text.

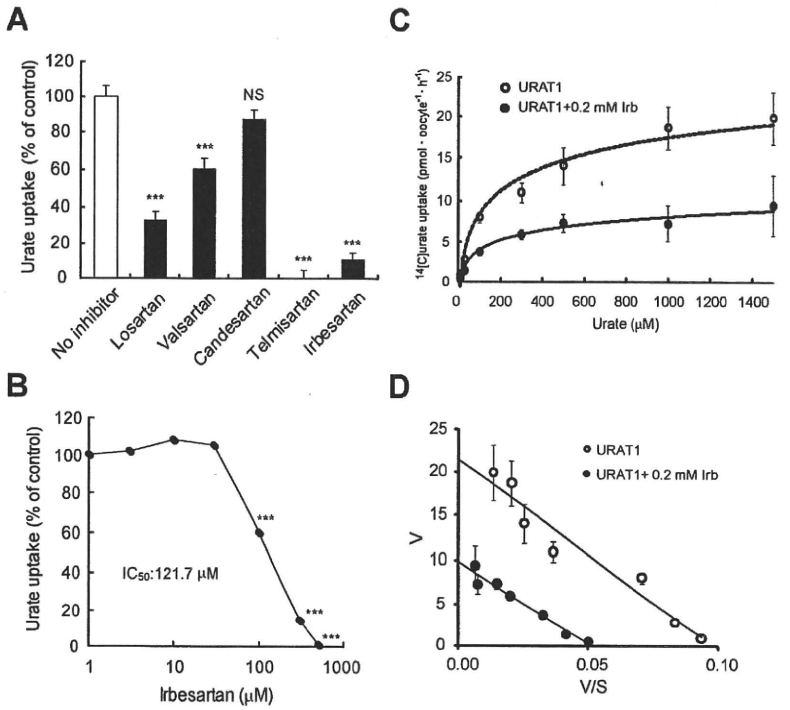

Fig. 2. The *cis*-inhibitory effect of irbesartan on URAT1-mediated uric acid uptake by URAT1-expressing oocytes. A: Uptake of [^{14}C]uric acid (20 μM) by URAT1-cRNA injected oocytes was measured in the presence or absence (no inhibitor) of ARBs [500 μM, except for telmisartan (300 μM)] for 1 h. B: Concentration-dependence of inhibition of urate uptake via URAT1 by irbesartan (1 – 500 μM). The URAT1-mediated uptake is expressed as percentage of the no-inhibitor control (absence of ARBs). C: The kinetic curve of urate uptake with 0.2 mM irbesartan. D: Eadie-Hofstee plot of URAT1-mediated urate uptake with 0.2 mM irbesartan. V/S, velocity per concentration of substrate; V, pmol·oocyte^{-1}·h^{-1}. Each data point is the mean ± S.E.M. from 3 independent experiments using 8 – 10 oocytes. ***$P < 0.001$, compared to the sample with no inhibitor. NS, not significant.

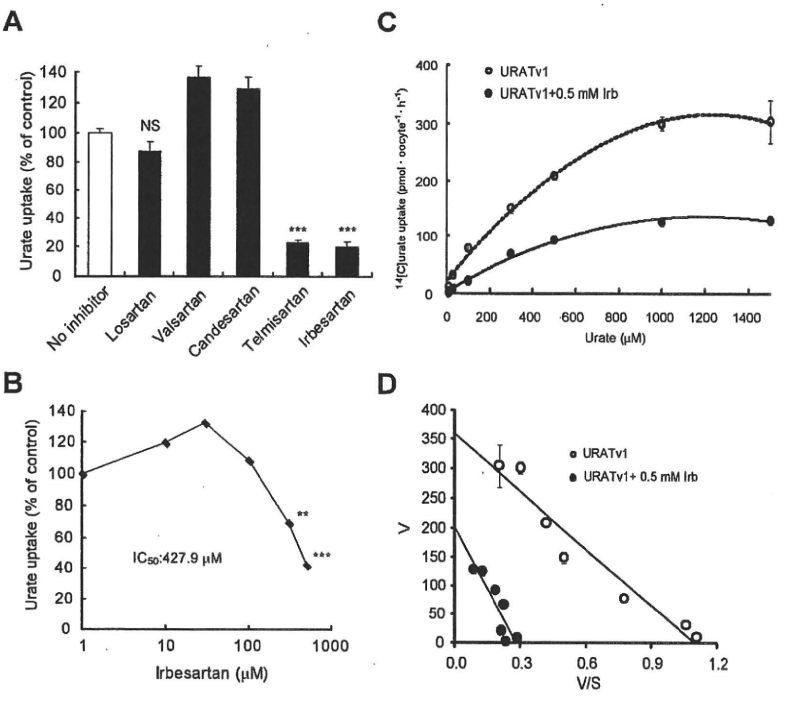

Fig. 3. The *cis*-inhibitory effect of irbesartan on URATv1-mediated uric acid uptake by URATv1-expressing oocytes. A: Uptake of [^{14}C]uric acid (20 μM) by URATv1-cRNA injected oocytes was measured in the presence or absence (no inhibitor) of ARBs [500 μM, except for telmisartan (300 μM)] for 1 h. B: Concentration-dependence of inhibition of urate uptake via URATv1 by irbesartan (1 – 500 μM). The URATv1-mediated uptake is expressed as percentage of the no-inhibitor control (absence of ARBs). C: The kinetic curve of urate uptake with 0.5 mM irbesartan. D: Eadie-Hofstee plot of URATv1-mediated urate uptake with 0.5 mM irbesartan. V/S, velocity per concentration of substrate; V, pmol·oocyte^{-1}·h^{-1}. Each data point is the mean ± S.E.M. from 3 independent experiments using 8 – 10 oocytes. **$P < 0.01$, ***$P < 0.001$, compared to the sample with no inhibitor. NS, not significant.

of irbesartan was almost 2 μM and it was lower than that of losartan (7 μM) (11, 12). This indicated that irbesartan may decrease SUA level from the luminal (apical) side because the drugs secreted into the tubular lumen will accumulate within the renal tubular system reaching a concentration exceeding that in plasma (13). Telmisartan, the other positive control, inhibited URAT1 and URATv1 to the same extent as irbesartan did. However, there is no indication that telmisartan enters the kidney (14) and therefore inhibition of renal UA reabsorption from the luminal side would seem to be unlikely. In addition, clinical data has shown no significant change in SUA in telmisartan-administered hypertensive patients (15), indicating that the inhibitory effect observed in vitro may not be relevant to in vivo UA transport in the kidney. Therefore irbesartan is likely to be a clinically more effective blocker of the renal UA transporter than telmisartan. In conclusion, our in vitro experiment demonstrated strong interaction of irbesartan with UA transporters, which exceeded that of losartan. Irbesartan could be used in hyperuricemic patients to decrease SUA level.

Acknowledgments

The authors thank Ms. A. Yamanishi for technical assistance. This work was supported in part by a Grant-in-Aid from the Japan Society for the Promotion of Science and grants from the Gout Research Foundation of Japan.

References

1 Messerli FH, Frohlich ED, Dreslinski GR, Suarez DH, Aristimuno GG. Serum uric acid in essential hypertension: an indicator of renal vascular involvement. Ann Intern Med. 1980;93:817–821.

2 Lin KC, Lin HY, Chou P. The interaction between uric acid level and other risk factors on the development of gout among asymptomatic hyperuricemic men in a prospective study. J Rheumatol. 2000;27:1501–1505.

3 Fauvel JP, Velon S, Berra N, Pozet N, Madonna O, Zech P, et al. Effects of losartan on renal function in patients with essential hypertension. J Cardiovasc Pharmacol. 1996;28:259–263.

4 Manolis AJ, Grossman E, Jelakovic B, Jacovides A, Bernhardi DC, Cabrera WJ, et al. Effects of losartan and candesartan monotherapy and losartan/hydrochlorothiazide combination therapy in patients with mild to moderate hypertension: Losartan Trial Investigators. Clin Ther. 2000;22:1186–1203.

5 Elliott WJ, Calhoun DA, DeLucca PT, Gazdick LP, Kerns DE, Zeldin RK. Losartan versus valsartan in the treatment of patients with mild to moderate essential hypertension: data from a multicenter, randomized, double-blind, 12-week trial. Clin Ther. 2001; 23:1166–1179.

6 Wurzner G, Gerster JC, Chiolero A, Maillard M, Fallab-Stubi CL, Brunner HR, et al. Comparative effects of losartan and irbesartan on serum uric acid in hypertensive patients with hyperuricaemia and gout. J Hypertens. 2001;19:1855–1860.

7 Enomoto A, Kimura H, Chairoungdua A, Shigeta Y, Jutabha P, Cha SH, et al. Molecular identification of a renal urate-anion exchanger that regulates blood urate levels. Nature (Lond). 2002; 417:447–452.

8 Anzai N, Ichida K, Jutabha P, Kimura T, Babu E, Jin CJ, et al. Plasma urate level is directly regulated by a voltage-driven urate efflux transporter URATv1 (SLC2A9) in humans. J Biol Chem. 2008;283:26834–26838.

9 Ichida K, Hosoyamada M, Hisatome I, Enomoto A, Hikita M, Endo H, et al. Clinical and molecular analysis of patients with renal hypouricemia in Japan: influence of URAT1 gene on urinary urate excretion. J Am Soc Nephrol. 2004;15:164–173.

10 Blumer J, Batisky DL, Wells T, Shi V, Solar-Yohay S, Sunkara G. Pharmacokinetics of valsartan in pediatric and adolescent subjects with hypertension. J Clin Pharmacol. 2009;49:235–241.

11 Goldberg MR, Bradstreet TE, McWilliams EJ, Tanaka WK, Lipert S, Bjornsson TD, et al. Biochemical effects of losartan, a nonpeptide angiotensin II receptor antagonist, on the renin-angiotensin-aldosterone system in hypertensive patients. Hypertension. 1995;25:37–46.

12 Sica DA, Marino MR, Hammett JL, Ferreira I, Gehr TWB, Ford NF. The pharmacokinetics of irbesartan in renal failure and maintenance hemodialysis. Clin Pharmacol Ther. 1997;62:610–618.

13 Anzai N, Kanai Y, Endou H. Organic anion transporter family: current knowledge. J Pharmacol Sci. 2006;100:411–426.

14 Stangier J, Schmid J, Turck D, Switek H, Verhagen A, Peeters PAM, et al. Absorption, metabolism, and excretion of intravenously and orally administered [^{14}C] telmisartan in healthy volunteers. J Clin Pharmacol. 2000;40:1312–1322.

15 Aranda P, Segura J, Ruilope LM, Aranda FJ, Frutos MA, López V, et al. Long-term renoprotective effects of standard versus high doses of telmisartan in hypertensive nondiabetic nephropathies. Am J Kid Dis. 2005;46:1074–1079.

Journal of Chromatography B, 878 (2010) 417–422

Contents lists available at ScienceDirect

Journal of Chromatography B

journal homepage: www.elsevier.com/locate/chromb

Analysis of [$^2H_7$]methionine, [$^2H_4$]methionine, methionine, [$^2H_4$]homocysteine and homocysteine in plasma by gas chromatography–mass spectrometry to follow the fate of administered [$^2H_7$]methionine

Yoshihiko Shinohara*, Hiroshi Hasegawa, Tomoyoshi Kaneko, Yuka Tamura, Takao Hashimoto, Kimiyoshi Ichida

Department of Pathophysiology, School of Pharmacy, Tokyo University of Pharmacy and Life Sciences, 1432-1 Horinouchi, Hachioji, Tokyo 192-0392, Japan

ARTICLE INFO

Article history:
Received 10 July 2009
Accepted 9 December 2009
Available online 22 December 2009

Keywords:
GC–MS
Stable isotope
Methionine
Homocysteine
Pharmacokinetics

ABSTRACT

Homocysteine plays a key role in several pathophysiological conditions. To assess the methionine–homocysteine kinetics by stable isotope methodology, we developed a simultaneous quantification method of [$^2H_7$]methionine, [$^2H_4$]methionine, methionine, [$^2H_4$]homocysteine and homocysteine in rat plasma by gas chromatography–mass spectrometry (GC–MS). [^{13}C]Methionine and [^{13}C]homocysteine were used as analytical internal standards to account for losses associated with the extraction, derivatization and chromatography. For labeled and non-labeled homocysteine measurements, disulfide bonds between homocysteine and other thiols or proteins were reduced by dithiothreitol. The reduced homocysteine and methionine species were purified by cation-exchange chromatography and derivatized with isobutyl chlorocarbonate in water–ethanol–pyridine. Quantification was carried out by selected ion monitoring of the molecular-related ions of *N*(*O*,*S*)-isobutyloxycarbonyl ethyl ester derivatives on the chemical ionization mode. The intra- and inter-day precision of the assay was less than 6% for all labeled and non-labeled methionine and homocysteine species. The method is sensitive enough to determine pharmacokinetics of labeled methionine and homocysteine.

© 2009 Elsevier B.V. All rights reserved.

1. Introduction

A moderate increase in plasma homocysteine concentration is a risk factor for many pathologic conditions, including cardiovascular disease, congenital abnormalities and neurological disorders [1–5]. However, it remains controversial as to whether the increased risk is mediated directly by homocysteine or whether it may simply be acting as a marker for another metabolite.

Homocysteine is a sulfur non-protein amino acid produced by de-methylation of methionine through the intermediates *S*-adenosylmethionine and *S*-adenosylhomocysteine. Homocysteine is then either re-methylated by accepting methyl group from either betaine or 5-methyltetrahydrofolate to form methionine or catabolized irreversibly to form cystathionine. In the absence of renal impairment, hyperhomocysteinemia is caused either by genetic defects in the enzymes involved in homocysteine metabolism or nutritional deficiencies in vitamin cofactors [6]. To understand the mechanisms of plasma homocysteine elevation, it is necessary to quantitatively assess methionine transmethylation and homocysteine re-methylation and transsulfuration in hyperhomocysteinemic patients.

Stable isotope methodology has provided a useful tool for metabolic and pharmacokinetic investigations for endogenous compounds [7–9]. We previously developed a gas chromatography–mass spectrometry (GC–MS) method for determination of methionine and total homocysteine in plasma with good accuracy and precision by using stable isotopically labeled compounds as analytical internal standards [10]. Stable isotopically labeled methionine has been also used as a biological internal standard to investigate the pharmacokinetic behavior of exogenously administered methionine and the extent of homocysteine re-methylation [11,12]. After administration of [3,3,4,4,*S*-methyl-$^2H_7$]methionine ([$^2H_7$]methionine) to rats, the plasma concentrations of the exogenously administered methionine ([$^2H_7$]methionine), the de-methylated homocysteine ([$^2H_4$]homocysteine), and re-methylated methionine ([$^2H_4$]methionine) simultaneously with endogenous methionine and homocysteine were determined by the double isotope dilution method. The double isotope dilution method, however, required a couple of plasma samples at each time obtained after dosing. A known amount of either labeled or unlabeled compounds (metabolite) was added to only one of the sample as analytical internal standard, and was not added to another sample. Peak-area

* Corresponding author. Tel.: +81 42 676 5699; fax: +81 42 676 5686.
E-mail address: sinohara@toyaku.ac.jp (Y. Shinohara).

1570-0232/$ – see front matter © 2009 Elsevier B.V. All rights reserved.
doi:10.1016/j.jchromb.2009.12.020

ratios of the two samples were then measured to calculate the concentrations of endogenous and exogenous (labeled) compounds in biological fluids [13–15] (Suppl. 1). The double isotope dilution method is generally time-consuming and often leads to a drawback in accurate quantification of low levels of unlabeled and labeled substances in biological fluids.

The aim of the present study is to develop simultaneous quantification method of [$^2H_7$]methionine, [$^2H_4$]methionine, methionine, [$^2H_4$]homocysteine and homocysteine in plasma by GC–MS using [^{13}C]methionine and [$^{13}C_2$]homocystine as analytical internal standards.

2. Experimental

2.1. Chemicals and reagents

DL-[3,3,4,4-$^2H_4$]Methionine ([$^2H_4$]methionine; >99% atom ^{2}H) and DL-[3,3,3′,3′,4,4,4′,4′-$^2H_8$]homocystine ([$^2H_8$]homocystine; 97.9% atom ^{2}H) were purchased from CDN isotopes (Quebec, Canada). DL-[1-^{13}C]Methionine ([^{13}C]methionine) was purchased from Isotec (Miamisburg, OH, USA). L-[$^2H_7$]Methionine was synthesized in our laboratory as described previously [15]. The isotopic purity and the enantiomeric purity were 99.3% atom ^{2}H and >99.8% enantiomeric excess, respectively. L-Methionine, isobutyl chlorocarbonate and dithiothreitol were purchased from Wako (Osaka, Japan). L-Homocystine was purchased from Nacalai Tesque (Kyoto, Japan). A strong cation-exchange solid-phase extraction column BondElut SCX (H^+ form, size 1 ml/100 mg) was purchased from Varian (Harbor City, OH, USA). All other chemicals and solvents were of analytical-reagent grade and were used without further purification.

2.2. Synthesis of [1,1′-$^{13}C_2$]homocystine

To a solution of [^{13}C]methionine (1.0 g, 6.6 mmol) in liquid ammonia (ca. 100 ml) were added small pieces of metallic lithium (180 mg) at −78 °C. The resulting blue solution was stirred at −78 °C with progress of the reaction being monitored by ^{1}H NMR as follows: aliquots of the solution (ca. 1 ml) were removed, evaporated and re-dissolved in 0.1 M sodium deuteroxide in deuterium oxide, and the disappearance of the S-CH_3 proton signal (δ 2.01 ppm) of unreacted DL-[1-^{13}C]methionine was monitored. Additional amounts of lithium were added in two portions (30 mg each) at 2 h intervals. After being stirred for 6 h, ammonium chloride (1 g) was added to the reaction mixture and the color of the solution was discharged. The solution was allowed to stand at room temperature to remove ammonia. The remaining off-white residue was dissolved in water (30 ml) and a continuous stream of oxygen was bubbled into the solution for 1 h. The pH of the solution was adjusted with 1 M HCl to pH 7 followed by standing overnight at 4 °C. The precipitate was collected by filtration, washed with cold H_2O, and dried to obtain [1,1′-$^{13}C_2$]homocystine ([$^{13}C_2$]homocystine) as a colorless solid (0.6 g, 32.8%). Elemental analysis, Calculated for $C_6{}^{13}C_2H_{16}N_2O_4S_2$: C, 35.54; H, 5.97; N, 10.36%. Found: C, 35.54; H, 5.90; N, 10.30%.

2.3. Gas chromatography–mass spectrometry-selected ion monitoring (GC–MS-SIM)

GC–MS-SIM analysis was made with a Shimadzu (Kyoto, Japan) QP2010 quadrupole GC–MS equipped with a data-processing system. A methylsilicone bonded-phase fused-silica capillary column SPB-1 (15 m × 0.25 mm i.d.) with a 0.25 μm film thickness (Supelco, Bellefonte, PA, USA) was connected directly to the ion source. Helium was used as the carrier gas at a column head pressure 100 kPa and total column flow-rate was maintained at 1.0 ml/min. A split–splitless injection system Shimadzu SPL-G9 was operated in the splitless mode with a purge flow-rate of 3 ml/min after 2 min. The initial column temperature was set 120 °C. After the sample injection, it was maintained for 2 min, increased at 30 °C/min to 270 °C and held at 270 °C for 1 min. The temperature of the injector was 250 °C. The mass spectrometer was operated in chemical ionization mode with isobutane as the reactant gas at an electron energy of 70 eV and an emission current of 60 μA. The ion source temperature was 280 °C. SIM was performed on the protonated molecular ions at *m/z* 278, 279, 282 and 285 for the *N(O,S)*-isobutyloxycarbonyl ethyl ester (IBC-OEt) derivatives of methionine, [^{13}C]methionine, [$^2H_4$]methionine and [$^2H_7$]methionine, respectively, and *m/z* 364, 365 and 368 for the IBC-OEt derivatives of homocysteine, [^{13}C]homocysteine and [$^2H_4$]homocysteine, respectively.

2.4. Preparation of standards

Stock solutions of methionine (1.53 mg/10 ml), [^{13}C]methionine (3.66 mg/25 ml), [$^2H_4$]methionine (1.57 mg/10 ml), [$^2H_7$]methionine (1.62 mg/10 ml), homocystine (2.63 mg/10 ml), [$^{13}C_2$]homocystine (2.73 mg/10 ml) and [$^2H_8$]homocystine (10.02 mg/10 ml) were prepared in 25 mM hydrochloric acid. The stock solutions were further diluted with 25 mM hydrochloric acid to prepare the standard solutions for calibration curve. Quality control (QC) standard solutions were prepared in the same manner as the calibration standard solutions. Storage of these solutions at 4 °C did not result in any detectable decomposition for more than 3 months.

2.5. Sample preparation for GC–MS-SIM

The protocol was based on an analytical procedure developed by our group [10]. To 50 μl of plasma were added 4.88 nmol of [^{13}C]methionine and 0.51 nmol of [$^{13}C_2$]homocystine as the internal standards dissolved in 0.2 ml of 25 mM hydrochloric acid. Following addition of 0.1 M sodium hydroxide (0.1 ml) and 1% dithiothreitol in acetonitrile (50 μl), the resulting solution was kept at room temperature for 30 min. The sample was deproteinized with 10% trichloroacetic acid (0.2 ml). After centrifugation at 1000 × *g* for 5 min at 4 °C, the supernatant was applied to a BondElut SCX cartridge, which was pre-washed and activated with 3 ml of methanol, 3 ml of a mixture of methanol–0.1 M hydrochloric acid (1:1, v/v) and 3 ml of 0.1 M hydrochloric acid. The cartridge was washed with 1 ml of water and 1 ml of a mixture of water–ethanol (2:1, v/v), and then eluted with 0.5 ml of a mixture of water–ethanol–pyridine (30:16:4, v/v). To the eluent was added isobutyl chlorocarbonate (50 μl) and the solution was mixed on a vortex for 10 s. The sample was extracted with 1 ml of chloroform. After evaporating to dryness under a stream of nitrogen, the residue was dissolved in 20 μl of ethyl acetate. A 0.2–2.0 μl portion of the solution was subjected to GC–MS-SIM.

2.6. Calibration curves and quantification

Each standard solution containing known amounts of methionine (0.51–3.06 nmol/50 μl 25 mM hydrochloric acid), [$^2H_4$]methionine (0.011–5.288 nmol/50 μl 25 mM hydrochloric acid), [$^2H_7$]methionine (0.010–10.102 nmol/50 μl 25 mM hydrochloric acid), homocystine (0.101–0.404 nmol/50 μl 25 mM hydrochloric acid), [$^2H_8$]homocystine (0.005–5.021 nmol/50 μl 25 mM hydrochloric acid) was added to 50 μl portions of rat blank plasma containing endogenous methionine and homocysteine. [^{13}C]methionine (4.88 nmol) and [$^{13}C_2$]homocystine (0.51 nmol) were added to the samples as internal standards. The samples were purified, derivatized and analyzed as described above. After

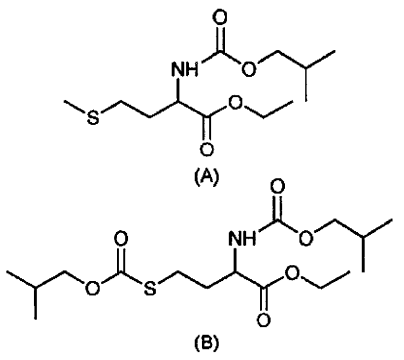

Fig. 1. Structures of *N*(*O*,*S*)-isobutyloxycarbonyl ethyl ester derivatives of methionine (A) and homocysteine (B).

correcting the peak-area values with the values of mutual contributions as shown Table 1, the peak-area ratios (*m*/*z* 278, *m*/*z* 282 and *m*/*z* 285 to *m*/*z* 279 for methionine species and *m*/*z* 364 and *m*/*z* 368 to *m*/*z* 365 for homocysteine species) were determined. The curves were obtained by an unweighted least-squares linear fitting of the peak-area ratios versus the amounts added on each sample. Plasma concentrations of labeled compounds were calculated by comparing the peak-area ratios obtained from the unknown samples with those obtained from the standard mixtures. The concentrations of endogenous methionine and homocysteine were calculated for dividing the *y*-intercept by the slope of the calibration curves.

2.7. Accuracy and precision

QC samples were prepared by spiking the QC solution for methionine (0.51, 1.03, 2.05 nmol/50 μl 25 mM hydrochloric acid), [$^2H_4$]methionine (0.010, 0.103, 1.027 nmol/50 μl 25 mM hydrochloric acid), [$^2H_7$]methionine (0.010, 0.101, 1.010 nmol/50 μl 25 mM hydrochloric acid), homocystine (0.10, 0.20, 0.30 nmol/50 μl 25 mM hydrochloric acid), [$^2H_8$]homocystine (0.005, 0.050, 0.501 nmol/50 μl 25 mM hydrochloric acid) into 50 μl aliquot of rat pooled plasma containing endogenous methionine and homocysteine. Following the addition of [^{13}C]methionine (4.88 nmol) and [$^{13}C_2$]homocystine (0.51 nmol) as internal standards, the samples were subjected to clean-up according to the procedure described above. The samples were analyzed by GC–MS-SIM and the peak-area ratios were measured.

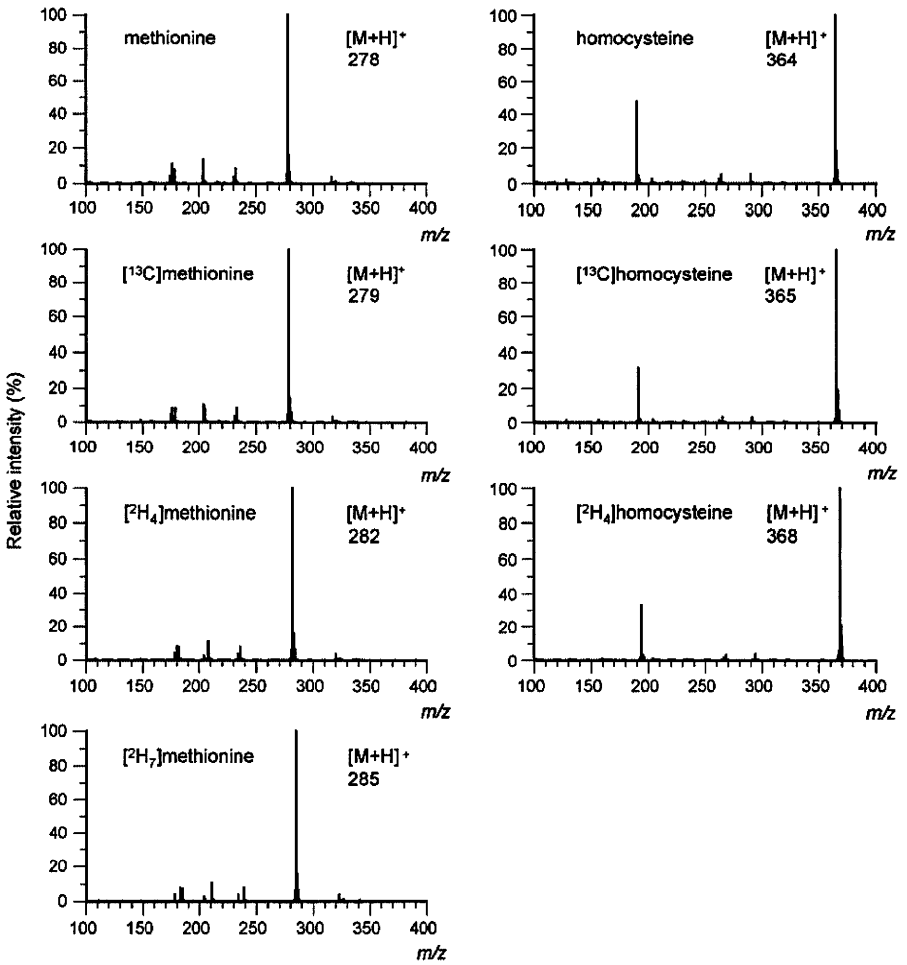

Fig. 2. Chemical ionization mass spectra of *N*(*O*,*S*)-isobutyloxycarbonyl ethyl ester derivatives of methionine, [^{13}C]methionine, [$^2H_4$]methionine, [$^2H_7$]methionine, homocysteine, [^{13}C]homocysteine and [$^2H_4$]homocysteine.

Table 1
Mutual contributions to ion intensity of various species in the channels monitored.

Compound	*m/z* 278	*m/z* 279	*m/z* 282	*m/z* 285
Methionine	100	14.918	0.117	0.023
[^{13}C]Methionine	4.247	100	0.701	0.029
[$^{2}H_4$]Methionine	0.052	0.145	100	0.803
[$^{2}H_7$]Methionine	0.025	0.149	0.961	100

Compound	*m/z* 364	*m/z* 365	*m/z* 368
Homocysteine	100	19.136	0.169
[^{13}C]Homocysteine	2.348	100	1.074
[$^{2}H_4$]Homocysteine	0.055	0.147	100

2.8. Dose experiment

After an overnight fast, male Sprague–Dawley rats ($n = 5$) aged 8 weeks, weighing 240–330 g, were anesthetized with pentobarbital (50 mg/kg body wt., i.p.). Each rat then received into the i.v. bolus injection of [$^{2}H_7$]methionine (30 μmol/kg weight) dissolved in saline (12.5 mg of [$^{2}H_7$]methionine/ml). Heparinized blood samples (150 μl) were obtained from the jugular vein at 5 min before and 0.5, 1, 3, 5, 10, 15, 20, 30, 45, 60, 90, 120, 180, 240 and 300 min after dosing. Plasma was separated and stored at −20 °C until analysis.

3. Results and discussion

One of the unique advantages for use of a stable isotope-labeled compound as a biological internal standard is that an endogenous compound and its exogenous administered labeled analog can be measured separately using GC–MS. The endogenous and exogenous compounds and their metabolites in biological fluids are often analyzed by using the double isotope dilution method. Since the method requires a couple of plasma samples at each time after the administration of labeled compound, it is necessary to collect relatively large volume of blood. Consequently, it is difficult to perform pharmacokinetic studies in small laboratory animals without complications of significant blood loss. This let us to use another type of stable isotopically labeled methionine and homocysteine as analytical internal standards for GC–MS-SIM.

A commercially available [^{13}C]methionine was chosen for an analytical internal standard for determination of methionine, [$^{2}H_4$]methionine and [$^{2}H_7$]methionine. [$^{13}C_2$]Homocystine was prepared from [^{13}C]methionine, and was used for an analytical standard for determination of homocysteine and [$^{2}H_4$]homocysteine.

Homocysteine is a sulfur amino acid with a thiol group that makes it susceptible to oxidation at physiological pH, thereby forming disulfides with other thiols. In plasma, only 1–2% occurs as the reduced form of homocysteine, leaving the remaining 98% in the form of oxidized homocysteine, i.e. in the form of disulfides [16]. Of these, about 75% is bound to protein (mainly albumin), the remainder occurs as non-protein bound disulfides. Moreover, it is known that a redistribution of homocysteine moieties occurs during storage of plasma [17]. To avoid these problems, plasma homocysteine has been measured after reduction of disulfide bonds. The total homocysteine, therefore, is the sum of all forms of homocysteine that exist in plasma [18]. In this study, after the reduction of the disulfide bond with dithiothreitol, the liberated homocysteine and [$^{2}H_4$]homocysteine were determined.

Following deproteinization with trichloroacetic acid and purification by cation-exchange chromatography using a BondElut SCX cartridge, the eluent in a mixture of water–ethanol–pyridine was added to isobutyl chlorocarbonate to form the IBC-OEt derivatives (Fig. 1) as described previously [10]. Fig. 2 shows the chemical ionization (CI) mass spectra of the derivatives of methionine, [^{13}C]methionine, [$^{2}H_4$]methionine, [$^{2}H_7$]methionine, homocysteine, [^{13}C]homocysteine and [$^{2}H_4$]homocysteine. Since IBC-OEt derivatives of methionine, [^{13}C]methionine, [$^{2}H_4$]methionine and [$^{2}H_7$]methionine gave strong protonated molecular ions $[M+H]^+$ at *m/z* 278, 279, 282 and 285, respectively, we have chosen these ions as the monitoring ions. The respective protonated molecular ion at *m/z* 364, 365 and 368 for the IBC-OEt derivatives of homocysteine, [^{13}C]homocysteine and [$^{2}H_4$]homocysteine were also observed in the relatively high intensities and were chosen for quantification by the SIM method.

It was expected that the IBC-OEt derivative of unlabeled methionine would have a significant contribution to the [M+H]+1 (*m/z* 279) because of the natural abundance of ^{2}H and ^{13}C. In addition, there is also the possibility that the derivative of [^{13}C]methionine could contribute to the [M+H]−1 (*m/z* 278), [M+H]+3 (*m/z* 282) and/or [M+H]+6 (*m/z* 285) peaks. The derivative of [$^{2}H_4$]methionine could contribute to the *m/z* 278, 279 and/or 285 peaks, and the derivative of [$^{2}H_7$]methionine could contribute to the *m/z* 278, 279 and/or 282 peaks. Similarly, the mutual contribution to ion intensities of various species in channels monitored (*m/z* 364, 365, 368) would be also expected for the derivatives of homocysteine, [^{13}C]homocysteine and [$^{2}H_4$]homocysteine. Pure sample of methionine, [^{13}C]methionine, [$^{2}H_4$]methionine, [$^{2}H_7$]methionine, homocysteine, [^{13}C]homocysteine and [$^{2}H_4$]homocysteine were analyzed by GC–MS-SIM and the relative peak intensities are summarized in Table 1. [$^{2}H_4$]Methionine, [$^{2}H_7$]methionine and [$^{2}H_4$]homocysteine possessed sufficiently high isotopic purity and the contributions to the other ions were minor. [^{13}C]Methionine and [^{13}C]homocysteine contain 4.2% and 2.3% of unlabeled analogous, respectively. The contributions of [M+H]+1 peak to mass spectra of unlabeled methionine and homocysteine are relatively large, 14.9% and 19.1%, respectively. Peak intensities are corrected using the values in Table 1 by the equations described previously [19].

Several different calibration curves were prepared in order to evaluate the amount of internal standards. When a little large amount of [^{13}C] compounds to unlabeled compounds was used, good accuracy and precise were observed. Plasma levels of endogenous methionine and total homocysteine were almost constant (2.93–2.97 nmol/50 μl for methionine, 0.19–0.21 nmol/50 μl for total homocysteine) after a bolus intravenous administration of [$^{2}H_7$]methionine (30 μmol/kg weight) into rats [11]. Therefore, 5 nmol of [^{13}C] methionine and 0.5 nmol of [$^{13}C_2$] homocystine per 50 μl of plasma were chosen for subsequent experiments.

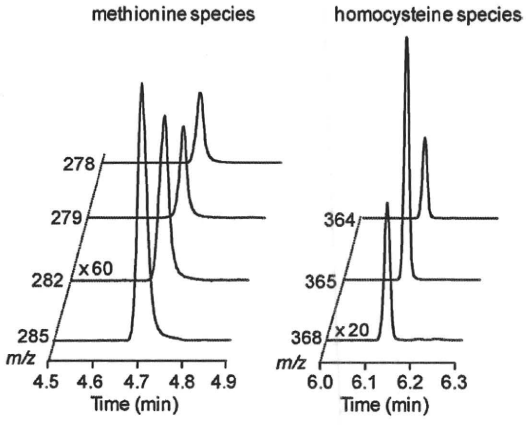

Fig. 3. Representative SIM profiles of rat plasma sample.

Table 2
Intra- and inter-day precision (R.S.D.) and accuracy (R.E.) for the determination of [$^2H_7$]methionine, [$^2H_4$]methionine, methionine, [$^2H_4$]homocysteine and homocysteine spiked to rat plasma.

Spiked (nmol)	Expected (nmol/ml)	Found (mean ± S.D.) (nmol/ml)	R.S.D. (%)	R.E. (%)
Intra-day (n = 3)				
[$^2H_7$]Methionine				
0.01	0.20	0.21 ± 0.01	4.35	5.73
0.10	2.02	2.08 ± 0.04	2.10	3.16
1.01	20.21	19.72 ± 1.36	6.89	−2.41
[$^2H_4$]Methionine				
0.01	0.21	0.20 ± 0.01	3.45	−1.15
0.10	2.05	2.06 ± 0.10	4.67	0.19
1.03	20.54	20.33 ± 0.28	1.36	−1.00
Methionine				
–	–	41.87 ± 0.70	1.67	–
0.51	51.54	51.25 ± 0.14	0.27	−0.56
1.03	61.80	61.07 ± 0.37	0.61	−1.18
2.05	82.34	82.70 ± 0.71	0.86	0.44
[$^2H_4$]Homocysteine				
0.01	0.20	0.20 ± 0.01	3.48	0.58
0.10	2.00	2.00 ± 0.05	2.31	−0.41
1.00	20.03	20.30 ± 0.16	0.81	1.33
Homocysteine				
–	–	7.88 ± 0.05	0.63	–
0.20	11.74	11.63 ± 0.05	0.43	−0.93
0.39	15.66	15.64 ± 0.14	0.90	−0.14
0.59	19.79	19.74 ± 0.20	1.01	0.80
Inter-day (n = 3)				
[$^2H_7$]Methionine				
0.01	0.20	0.20 ± 0.01	4.87	0.51
0.10	2.02	2.10 ± 0.07	3.19	3.84
1.01	20.21	20.52 ± 0.23	1.11	1.57
[$^2H_4$]Methionine				
0.01	0.21	0.21 ± 0.00	1.93	0.87
0.10	2.05	2.07 ± 0.02	0.72	0.99
1.03	20.54	20.43 ± 0.08	0.41	−0.53
Methionine				
–	–	41.88 ± 1.04	2.48	–
0.51	51.54	51.19 ± 0.05	0.10	−0.67
1.03	61.80	61.48 ± 0.35	0.57	−0.53
2.05	82.34	83.11 ± 0.41	0.57	0.94
[$^2H_4$]Homocysteine				
0.01	0.20	0.20 ± 0.01	2.53	−1.09
0.10	2.00	1.99 ± 0.03	1.56	−0.70
1.00	20.03	20.10 ± 0.39	1.94	0.36
Homocysteine				
–	–	7.74 ± 0.15	1.94	–
0.20	11.74	11.59 ± 0.04	0.35	−1.28
0.39	15.66	15.58 ± 0.13	0.83	−0.51
0.59	19.58	19.74 ± 0.19	0.96	0.82

Calibration curves were prepared from a series of samples containing various amounts of methionine, [$^2H_4$] methionine, [$^2H_7$]methionine, homocysteine and [$^2H_4$]homocysteine. When the peak-area ratios were plotted against the amounts added, linearity was excellent over the respective calibration ranges, with corresponding correlation coefficients (R^2) consistently >0.99 for all compounds.

The lower limit of quantification (LOQ) for the present method was determined by spiking 50 μl aliquots rat plasma with [$^2H_7$]methionine, [$^2H_4$]methionine and [$^2H_8$]homocystine. When a relative standard deviation of 10% or greater was used as a criterion for an LOQ [19], the values for [$^2H_7$]methionine, [$^2H_4$]methionine and [$^2H_4$]homocysteine were around 0.085, 0.085 and 0.080 nmol/ml plasma, respectively. The precision and accuracy of the assay were determined by spiking 50 μl-aliquots of blank rat plasma with the QC solutions. The results are presented in Table 2. The estimated amounts were in good agreement with the actual amounts added. The intra- and inter-day precision of the assay was less than 6% for each amino acid at all concentrations. The results demonstrated an excellent reproducibility. In the previously developed double isotope dilution method, the intra-day precisions of 2 nmol/ml plasma were 10.2%, 7.3% and 11.9% for [$^2H_7$]methionine, [$^2H_4$]methionine and [$^2H_4$]homocysteine, respectively (unpublished data). The values of 0.2 nmol/ml plasma were greater than 20% for each amino acid. The present method uses a lower blood sample volume and shows lower variation than the double isotope dilution method.

The present GC–MS-SIM method was applied for the quantification of plasma concentration of [$^2H_7$]methionine, [$^2H_4$]methionine, methionine, total [$^2H_4$]homocysteine and total homocysteine after intravenous administration of [$^2H_7$]methionine (30 μmol/kg weight) to Sprague–Dawley male rats. Representative SIM profiles of plasma samples are shown in Fig. 3. There was no interference from endogenous compounds in the vicinity of the peaks of

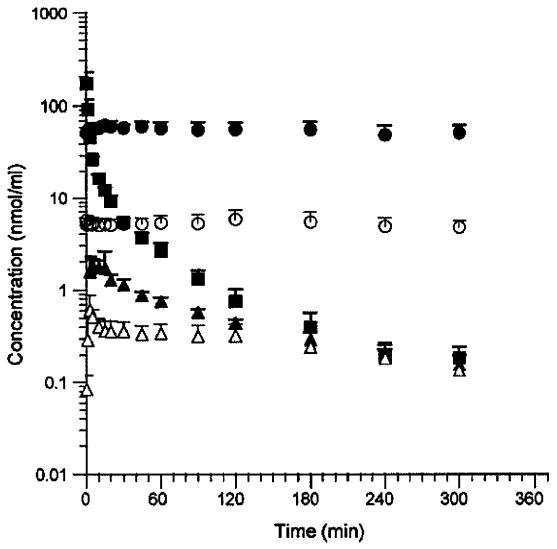

Fig. 4. Semi-logarithmic plots of plasma concentration versus time curves of [$^2H_7$]methionine (■), [$^2H_4$]methionine (▲), methionine (●), total [$^2H_4$]homocysteine (□) and total homocysteine (○) in rats ($n = 5$) after an intravenous administration of [$^2H_7$]methionine (30 μmol/kg weight).

analyses in the SIM. Plasma concentrations of [$^2H_7$]methionine, [$^2H_4$]methionine and total [$^2H_4$]homocysteine with endogenous methionine and total homocysteine could be followed up to 5 h (Fig. 4). Pharmacokinetic studies of [$^2H_7$]methionine or [$^2H_4$]methionine are now in progress and will be described in detail.

4. Conclusions

By using [^{13}C]methionine and [$^{13}C_2$]homocystine as analytical internal standards, the present method provides a sensitive and reliable technique for the simultaneous determination of [$^2H_7$]methionine, [$^2H_4$]methionine and [$^2H_4$]homocysteine with endogenous methionine and homocysteine in plasma with good accuracy and precision. The method can be applied to pharmacokinetic and metabolic studies with a particular interest in the re-methylation of homocysteine to methionine.

Acknowledgment

This work was supported in part by a grant for Private Universities provided by the Promotion and Mutual Aid Corporation for Private Schools of Japan.

Appendix A. Supplementary data

Supplementary data associated with this article can be found, in the online version, at doi:10.1016/j.jchromb.2009.12.020.

References

[1] G.N. Welch, J. Loscalzo, N. Engl. J. Med. 338 (1998) 1042.
[2] J. Townend, J. O'Sullivan, J.T. Wilde, Blood Rev. 12 (1998) 23.
[3] S.E. Vollset, H. Refsum, L.M. Irgens, B.M. Emblem, A. Tverdal, H.K. Gjessing, A.L.B. Monsen, P.M. Ueland, Am. J. Clin. Nutr. 71 (2000) 962.
[4] K. Nilsson, L. Gustafson, R. Faldt, A. Andersson, L. Brattstrom, A. Lindgren, B. Israelsson, B. Hultberg, Eur. J. Clin. Invest. 26 (1996) 853.
[5] S. Seshadri, A. Beiser, J. Selhub, P.F. Jacques, I.H. Rosenberg, R.B. D'Agostino, P.W.F. Wilson, P.A. Wolf, N. Engl. J. Med. 346 (2002) 476.
[6] G.J. Hankey, J.W. Eikelboom, Lancet 354 (1999) 407.
[7] T.A. Baillie, Pharmacol. Rev. 33 (1981) 81.
[8] Y. Shinohara, S. Baba, Steroids 55 (1990) 170.
[9] H. Hasegawa, T. Matsukawa, Y. Shinohara, R. Konno, T. Hashimoto, Am. J. Physiol. Endocrinol. Metab. 287 (2004) E160.
[10] Y. Shinohara, H. Hasegawa, K. Tagoku, T. Hashimoto, J. Chromatogr. B 758 (2001) 283.
[11] Y. Shinohara, H. Hasegawa, K. Tagoku, T. Hashimoto, Life Sci. 70 (2001) 727.
[12] Y. Shinohara, H. Hasegawa, K. Ogawa, K. Tagoku, T. Hashimoto, Metabolism 55 (2006) 899.
[13] S. Baba, Y. Shinohara, Y. Kasuya, J. Clin. Endocrinol. Metab. 50 (1980) 889.
[14] Y. Kasuya, H. Ishimaru, H. Shibasaki, T. Furuta, Steroids 63 (1998) 122.
[15] H. Hasegawa, Y. Shinohara, K. Tagoku, T. Hashimoto, J. Labelled Compd. Radiopharm. 44 (2001) 21.
[16] P.M. Ueland, Clin. Chem. 41 (1995) 340.
[17] P.M. Ueland, H. Refsum, S.P. Stabler, M.R. Malinow, A. Andersson, R.H. Allen, Clin. Chem. 39 (1993) 1764.
[18] H. Refsum, A.D. Smith, P.M. Ueland, E. Nexo, R. Clarke, J. McPartlin, C. Johnston, F. Engbaek, J. Schneede, C. McPartlin, J.M. Scott, Clin. Chem. 50 (2004) 3.
[19] H. Hasegawa, Y. Shinohara, T. Hashimoto, R. Matsuda, Y. Hayashi, J. Chromatogr. A 1136 (2006) 226.

0090-9556/10/3812-2320–2328$20.00
DRUG METABOLISM AND DISPOSITION
Copyright © 2010 by The American Society for Pharmacology and Experimental Therapeutics
DMD 38:2320–2328, 2010

Vol. 38, No. 12
34603/3646104
Printed in U.S.A.

Receptor for Activated C-Kinase 1 Regulates the Cell Surface Expression and Function of ATP Binding Cassette G2[S]

Yuki Ikebuchi, Kousei Ito, Tappei Takada, Naohiko Anzai, Yoshikatsu Kanai, and Hiroshi Suzuki

Department of Pharmacy, The University of Tokyo Hospital, Faculty of Medicine, The University of Tokyo, Tokyo, Japan (Y.I., K.I., T.T., H.S.); Department of Pharmacology and Toxicology, Kyorin University School of Medicine, Tokyo, Japan (N.A.); and Department of Pharmacology, Graduate School of Medicine, Osaka University, Osaka, Japan (Y.K.)

Received May 20, 2010; accepted September 21, 2010

ABSTRACT:

In a previous report, we identified the receptor for activated C-kinase 1 (RACK1) as a positive regulator of the cellular localization and expression of ATP-binding cassette B4, a phosphatidylcholine translocator expressed on the bile canalicular membrane. In the present study, we focused on the role of RACK1 on ATP-binding cassette G2 (ABCG2), which is responsible for the cellular extrusion of compounds including antitumor drugs. Protein expression of ABCG2 was up-regulated by RACK1 overexpression, although mRNA expression of ABCG2 was not dependent on RACK1. The effect of RACK1 on the expression of ABCG2 on the cell surface was confirmed by the uptake of [^{3}H]estrone sulfate, an ABCG2 substrate, into isolated membrane vesicles. The expression of RACK1 affected cellular resistance to mitoxantrone, an anticancer drug excreted by ABCG2, and this effect of RACK1 was abolished in the presence of fumitremorgin C, a selective ABCG2 inhibitor. These results suggest that RACK1 has functional significance as a regulatory cofactor of ABCG2 and is indispensable for the cell surface expression and excretion function of ABCG2. The precise mechanism for RACK1-dependent expression of ABCG2 remains to be clarified, because the results of *N*-benzoyloxycarbonyl (*Z*)-Leu-Leu-leucinal (MG132) and chloroquine treatment and those of metabolic labeling experiments did not give us clear evidence whether the reduction of ABCG2 expression in RACK1-knocked down cells may be caused by the suppression of ABCG2 protein synthesis or by acceleration of its degradation.

Introduction

Several lines of evidence suggest that the cellular localization and expression of ATP-binding cassette (ABC) transporters are regulated by several cofactors (Ortiz et al., 2004; Minami et al., 2009). In a previous report, we used yeast two-hybrid screening to show that the receptor for activated C-kinase 1 (RACK1) is a novel binding partner of ABCB4, which is responsible for the biliary excretion of phospholipids (Ikebuchi et al., 2009). We found that down-regulation of endogenous RACK1 expression in HeLa cells by small interfering RNA (siRNA) resulted in the localization of ABCB4 in the cytosolic compartment and reduced protein expression of ABCB4. Consequently, ABCB4-mediated phosphatidylcholine translocation activity decreased significantly when endogenous RACK1 expression was suppressed in HeLa cells. These results suggested that RACK1 has functional significance as a regulatory cofactor of ABCB4.

RACK1 is a scaffold protein with seven WD-40 repeats and was originally identified based on its ability to bind to the activated protein kinase C (PKC) isoforms, particularly PKC-βII (Mochly-Rosen et al., 1991). RACK1 stabilizes activated PKC-βII and facilitates its trafficking within the cells to regulate the phosphorylation state of target proteins. Previous studies have also shown that RACK1 interacts with a range of different cellular proteins and, consequently, may be involved in diverse cellular processes, including signal transduction, cell growth, differentiation, and protein synthesis (McCahill et al., 2002). In addition, it has been established that cell surface expression of several transmembrane proteins such as cystic fibrosis transmembrane conductance regulator (CFTR/ABCC7) may be positively regulated by RACK1 in a direct or an indirect manner (Liedtke et al., 2002). In the present study, we also examined whether the cellular localization and expression of other ABC transporters are affected by the suppression of endogenous RACK1. ABCG2 was identified as a candidate transporter.

ABCG2 is responsible for multidrug resistance to a broad range of anticancer drugs, including mitoxantrone, topotecan, and 7-ethyl-10-

This work was supported in part by the Ministry of Education, Science and Culture of Japan [Grant-in-Aid 17081006 for Scientific Research on Priority Areas].

Article, publication date, and citation information can be found at http://dmd.aspetjournals.org.

doi:10.1124/dmd.110.034603.

[S] The online version of this article (available at http://dmd.aspetjournals.org) contains supplemental material.

ABBREVIATIONS: ABC, ATP-binding cassette; RACK1, receptor for activated C-kinase 1; siRNA, small interfering RNA; PKC, protein kinase C; SN-38, 7-ethyl-10-hydroxycamptothecin; E_1S, estrone sulfate; FTC, fumitremorgin C; LAMP1, lysosomal-associated membrane protein; PCR, polymerase chain reaction; MEM, minimum essential medium; FBS, fetal bovine serum; EGFP, enhanced green fluorescent protein; PBS, phosphate-buffered saline; miRNA, microRNA; RIPA, radioimmunoprecipitation assay; MG132, *N*-benzoyloxycarbonyl (*Z*)-Leu-Leu-leucinal; MTT, 3-(4,5-dimethylthiazol-2-yl)-2,5, diphenyltetrazolium bromide.

hydroxycamptothecin (SN-38) (Doyle et al., 1998; Haimeur et al., 2004). Knockout mice studies have shown that ABCG2 which is expressed in normal tissues, such as the gastrointestinal tract, liver, and mammary gland, and the blood-brain barrier, functions in the regulation of the disposition of exogenous compounds (Breedveld et al., 2005; Merino et al., 2005). In humans, *ABCG2* gene expression is associated with a poor response to remission-induction therapy in patients with acute myeloid leukemia treated with mitoxantrone (Steinbach et al., 2002). In addition, single nucleotide polymorphisms in the *ABCG2* gene affect its expression level and functional activity (Kondo et al., 2004) and, consequently, the clinical outcomes or the risk of adverse effects of treatment with anticancer drugs (Noguchi et al., 2009). Several factors involved in transcriptional regulation, including sex hormones (Imai et al., 2005), hypoxia (Krishnamurthy et al., 2004), and peroxisome proliferator-activated receptor γ (Szatmari et al., 2006) have been reported to regulate the transcription of ABCG2 (Robey et al., 2009). In addition, cytokines such as tumor necrosis factor-α and growth factors have been reported to affect the transcription of ABCG2, although the precise molecular mechanism has not been established (Evseenko et al., 2007). Compared with transcriptional regulation, information on post-transcriptional regulation of ABCG2 is limited. Mogi et al. (2003) reported that Akt-1 is involved in the surface expression of ABCG2 in hematopoietic stem cells and contributes to the formation of a side population (Mogi et al., 2003). In addition, we reported that phosphorylation of ABCG2 mediated by the phosphatidylinositol 3-kinase-Akt/protein kinase B pathway increases the apical surface expression of ABCG2 in LLC-PK1 cells (Takada et al., 2005a). In the present study, we examined the role of RACK1 in the post-transcriptional regulation of ABCG2.

Materials and Methods

Materials. [^{35}S]Methionine/cysteine cell labeling mix (NEG-772) and [^{3}H]estrone sulfate (E_1S) were purchased from PerkinElmer Life and Analytical Sciences (Waltham, MA). Mitoxantrone dihydrochloride was purchased from LKT Laboratories (St. Paul, MN). Fumitremorgin C (FTC) was purchased from Calbiochem (Darmstadt, Germany). Anti-ABCG2 rat monoclonal antibody (BXP-53) and anti-α-tubulin rabbit polyclonal antibody (ab15246) were purchased from Abcam Inc. (Cambridge, MA). Anti-ABCG2 mouse monoclonal antibody (5D3) was purchased from eBioscience (San Diego, CA). Anti-RACK1 mouse monoclonal IgM was purchased from Transduction Laboratories (San Jose, CA). Anti-Na^+/K^+-ATPase α rabbit polyclonal antibody (H-300), anti-calnexin goat polyclonal antibody (C-20), and anti-Rab5a rabbit polyclonal antibody (S-19) were purchased from Santa Cruz Biotechnology Inc. (Heidelberg, Germany). Anti-LAMP1 rabbit monoclonal antibody was purchased from Sigma-Aldrich (St. Louis, MO). BODIPY TR-labeled ceramide and Alexa 633-conjugated transferrin were purchased from Invitrogen (Tokyo, Japan). All other chemicals used were commercially available and of reagent grade.

Plasmid Construction. The human ABCG2 cDNA (GenBank accession number NM_004827) was constructed as described previously (Takada et al., 2005b). The full-length coding sequence of RACK1 cDNA (GenBank accession number NM_006098) was amplified by polymerase chain reaction (PCR) and the myc tag sequence (EQKLISEEDL) was added to the 5′-end, followed by subcloning into a pcDNA3.1 vector plasmid (Invitrogen). The sequences of all constructs were confirmed using an automatic DNA sequencer (ABI PRISM 377 DNA Sequencer; Applied Biosystems, Foster City, CA).

Cell Culture. HeLa cells (RIKEN, Ibaraki, Japan) were maintained in Eagle's minimum essential medium (MEM) (Nacalai Tesque, Kyoto, Japan) supplemented with 10% fetal bovine serum (FBS) (Biological Industries, Haemek, Israel), 100 units/ml penicillin and streptomycin (Invitrogen), and 1% nonessential amino acid (Invitrogen) at 37°C in a humidified atmosphere supplemented with 5% CO_2.

Transient Suppression of RACK1 Expression via RNA Interference. Suppression of RACK1 expression was accomplished using an siRNA duplex targeted to RACK1 mRNA (siRACK1) sequences. The siRACK1 sequences were 5′-CCAUCAAGCUAUGGAAUACTT-3′ (sense) and 5′-GUAUUCCAUAGCUUGAUGGTT-3′ (antisense) (Kiely et al., 2006). The negative control siRNA (siPerfect Negative Control; siControl) was designed not to affect the expression of any genes. These siRNAs were purchased from Sigma-Aldrich.

To examine the effect of siRNAs on the expression of RACK1, HeLa cells were seeded at a density of 1.0×10^5 cells per 12-well plates (0.25×10^5 cells/cm^2) and, simultaneously, siRACK1 or siControl was transfected into these cells using Lipofectamine RNAiMAX reagent (Invitrogen) according to the method recommended by the manufacturer. Seventy-two hours after siRNA transfection, RNA was isolated using RNA-Solv Reagent (Omega Bio-tek, Doraville, GA) according to the manufacturer's instructions, and then reverse transcription was performed by ReverTra Ace-α- (Toyobo, Tokyo, Japan). To quantify the mRNA expression levels, real-time quantitative PCR was performed using Brilliant SYBR Green QPCR Master Mix (Stratagene, La Jolla, CA) and the Chromo4 real-time PCR analysis system (Bio-Rad Laboratories, Hercules, CA) at 95°C for 10 min followed by 40 cycles at 95°C for 15 s, 50°C for 30 s, and 72°C for 40 s. The primers used for the quantification were as follows: 5′-GGAATACCCTGGGTGTGTGC-3′ (RACK1, sense) and 5′-GTTGAGATCCCATAACATGG-3′ (RACK1, antisense), 5′-GCATTCCACGATATGGATT-3′ (ABCG2, sense) and 5′-TCAGGTAGGCAATTGTGAG-3′ (ABCG2, antisense), and 5′-TTCAACACCCCAGCCATGTAGG-3′ (β-actin, sense) and 5′-GTGGTGGTGAAGCTGTAGCC-3′ (β-actin, antisense). The mRNA expression levels of RACK1 and ABCG2 were normalized by that of β-actin.

Immunohistochemical Staining. To identify the cellular localization of exogenous ABCG2, HeLa cells were seeded on glass-based 35-mm dishes at a density of 2×10^5 cells (0.22×10^5 cells/cm^2) and transfected with siRNAs against RACK1 using Lipofectamine RNAiMAX reagent. Then 24 h after siRNA transfection, these cells were transfected with enhanced green fluorescent protein (EGFP)-ABCG2 using FuGENE6 (Roche Applied Science, Indianapolis, IN). Cells were fixed with 100% methanol at −20°C for 10 min and washed three times with ice-cold phosphate-buffered saline (PBS). Each organellar marker was immunostained with the following primary antibodies: anti-calnexin antibody (100-fold diluted) as an endoplasmic reticulum marker, anti-LAMP1 antibody (200-fold diluted) as a lysosome marker, and anti-Rab5a antibody (100-fold diluted) as an early endosome marker. After cells were washed three times with PBS, they were incubated with the corresponding Alexa-conjugated secondary antibodies (Invitrogen) diluted 250-fold in PBS containing 0.1% bovine serum albumin at 37°C for 1 h. To stain the nucleus, cells were pretreated with 0.2 mg/ml RNaseA (Sigma-Aldrich) in PBS at room temperature for 10 min and incubated with TO-PRO-3 iodide (Invitrogen) diluted 250-fold in PBS at room temperature for 20 min. After cells were washing three times with PBS, they were mounted in Vectashield Mounting Medium (Vector Laboratories, Burlingame, CA). In addition, the Golgi apparatus and recycling endosome were stained with BODIPY TR-labeled ceramide and Alexa 633-conjugated transferrin following the manufacturer's instructions.

To examine the intracellular localization of endogenous ABCG2, cells were fixed with 4% paraformaldehyde at room temperature for 10 min with or without permeabilization treatment by 0.1% Triton X-100 at room temperature for 5 min. Endogenous ABCG2 was immunostained with two kinds of anti-ABCG2 primary antibodies, BXP-53 (50-fold diluted) and 5D3 (10-fold diluted), and the corresponding secondary antibodies. The cellular localization of the targeted proteins was visualized by confocal laser scanning microscopy (FV1000; Olympus, Tokyo, Japan).

Construction of Stable Cell Lines. Construction of stably knocked down HeLa cells was performed using lentivirus vectors as indicated by the manufacturer. In brief, lentiviruses carrying microRNA (miRNA) sequences were constructed using a BLOCK-iT Pol II RNAi Expression Vector Kit (Invitrogen) and a ViraPower Promoterless Lentiviral Expression System (Invitrogen). The following sequences were used as the targeting miRNA sequence: 5′-GTCTCCACGCGCAGTACATTT-3′ (miControl), 5′-CACTCCCACTTTGTTAGTGAT-3′ (miRACK1*1), 5′-TCAACGAAGGCAAACACCTTT-3′ (miRACK1*2), and 5′-CTCCTTCTGTCATCAACTCAG-3′ (miABCG2). Infected HeLa cells were selected using 3 μg/ml blasticidin (Invitrogen). The surviving cells were used as control cells (miControl cells),

stably RACK1-knocked down cells (miRACK1 cells) or stably ABCG2-knocked down cells (miABCG2 cells).

HeLa cells were transfected with myc-tagged RACK1 cDNA or pcDNA3.1 using FuGENE6 to construct RACK1 stably expressing and control HeLa cells, respectively, and cultured for 48 h. The prepared cells were cultured in MEM medium supplemented with 10% FBS, 100 units/ml penicillin and streptomycin, 1% nonessential amino acids, and 1 mg/ml G418 sulfate (Nacalai Tesque) for 2 weeks. Selected cells were isolated and their expression levels of RACK1 were confirmed by Western blotting.

Western Blot Analysis. Cells were lysed with RIPA buffer (0.1% SDS, 0.5% sodium deoxycholate, 1% Nonidet P-40, 2 mM phenylmethylsulfonyl fluoride, 5 μg/ml leupeptin, 1 μg/ml pepstatin, and 5 μg/ml aprotinin) at 4°C for 20 min. After centrifugation at 20,000g for 20 min, the supernatant was obtained, and the protein concentrations were determined by the method of Lowry et al. (1951). The specimens were subjected to Western blot analysis. The primary antibodies were anti-RACK1 antibody (500-fold diluted), anti-ABCG2 antibody (200-fold diluted), and anti-α-tubulin antibody (1000-fold diluted). Finally, the membranes were allowed to bind to horseradish peroxidase-labeled secondary antibodies (GE Healthcare, Little Chalfont, Buckinghamshire, UK) and detected with an ECL Plus Western Blotting Detection System (GE Healthcare) using a luminescent image analyzer (Bio-Rad Laboratories). The data are expressed as the mean ± S.D. of triplicate preparations.

Cell Surface Biotinylation Assay. ABCG2 expression on the plasma membrane was assessed using a biotinylation method described previously (Hayashi et al., 2005). In brief, cells were seeded at a density of 2.0×10^5 cells per six-well plates (0.25×10^5 cells/cm^2) 72 h before the assay. The prepared cells were washed twice with ice-cold PBS containing 0.1 mM $CaCl_2$ and 1 mM $MgCl_2$ (PBS-Ca/Mg) and incubated with 1 mg/ml NHS-SS-biotin (Pierce Biotechnology, Rockford, IL) at 4°C for 30 min. After removing the NHS-SS-biotin, the cells were washed with PBS-Ca/Mg containing 100 mM glycine and incubated at 4°C for 15 min, then disrupted with 250 μl of RIPA buffer at 4°C for 30 min. After centrifugation at 20,000g for 20 min, the supernatant was obtained and streptavidin-agarose beads (Pierce Biotechnology) were added to the lysate, followed by incubation at 4°C for 2 h with continuous gentle shaking. The beads were washed five times with RIPA buffer. The biotinylated proteins were eluted with 20 μl of SDS loading buffer at 60°C for 15 min. The biotinylated proteins and whole-cell lysate were subjected to Western blot analysis.

ABCG2 Protein Stability. In each assessment, miControl cells and miRACK1 cells were seeded 48 h before the assay at a density of 2×10^5 cells per six-well plates (0.22×10^5 cells/cm^2). Cycloheximide (Sigma-Aldrich), an inhibitor of protein translation, was added (100 μM), and cells were collected after 0, 10, 30, 60, 120, and 240 min. *N*-Benzoyloxycarbonyl (*Z*)-Leu-Leu-leucinal (MG132) (Calbiochem), a proteasomal degradation inhibitor, was added (5 μM) 48 h after cell seeding, and the cells were cultured for an additional 24 h. Chloroquine diphosphate (Nacalai Tesque), a lysosomal degradation inhibitor, was added (250 μM) 48 h after cell seeding, and the cells were cultured for an additional 6 h. The protein expression levels of endogenous ABCG2 in each specimen were examined by Western blot analysis as described above.

Metabolic Labeling of ABCG2. miControl cells and miRACK1 cells were incubated in methionine/cysteine-free MEM (Invitrogen) for 1 h just before the experiment. The cells were incubated in the labeling medium containing 100 μCi/ml [^{35}S]methionine/cysteine cell labeling mix and collected at 0, 10, 20, 30, 60, and 90 min. The cells were lysed with RIPA buffer and 0.5 μg of anti-ABCG2 monoclonal antibody (BXP-53) was added to immunoprecipitate endogenous ABCG2. The mixture was incubated overnight at 4°C with continuous gentle shaking. Immunoprecipitation was performed using magnetic beads coated with protein G (Ademtech, Pessac, France), and the immunoprecipitate was washed five times with RIPA buffer. Proteins bound to the protein G beads were eluted with 2× SDS loading buffer containing 50 mM dithiothreitol at 37°C for 1 h. The eluted specimens were separated by SDS-polyacrylamide gel electrophoresis and exposed to a Super Resolution PhosphorImager (PerkinElmer Life and Analytical Sciences). The radioactivity was detected using a Cyclone PhosphorImager (PerkinElmer Life and Analytical Sciences). ABCG2 expression was quantified and normalized by the expression level of total ABCG2 in miControl cells observed at 1 h. The results are given as the mean ± S.D. of triplicate determinations.

Preparation of Membrane Vesicles. Membrane vesicles were prepared from HeLa cells according to a method described previously (Kondo et al., 2004). In brief, the harvested cells were diluted 40-fold with hypotonic buffer (1 mM Tris-HCl and 0.1 mM EDTA, pH 7.4, at 4°C) and stirred gently for 1 h on ice in the presence of 2 mM phenylmethylsulfonyl fluoride, 5 μg/ml leupeptin, 1 μg/ml pepstatin, and 5 μg/ml aprotinin. The cell lysate was centrifuged at 100,000g for 30 min at 4°C, and the resulting pellet was suspended in 10 ml of isotonic TS buffer (10 mM Tris-HCl, pH 7.4, at 4°C, and 250 mM sucrose) and homogenized using a Dounce B homogenizer (glass/glass, tight pestle, 30 strokes). The crude membrane fraction was layered on top of a 38% (w/v) sucrose solution in 5 mM Tris-HEPES (pH 7.4 at 4°C) and centrifuged in a Beckman SW41 rotor at 280,000g for 45 min at 4°C. The turbid layer at the interface was collected, diluted to 23 ml with TS buffer, and centrifuged at 100,000g for 30 min at 4°C. The resulting pellet was suspended in 400 μl of TS buffer. Vesicles were formed by passing the suspension 30 times through a 25-gauge needle with a syringe. The membrane vesicles were finally frozen in liquid nitrogen and stored at −80°C until use.

Transport Study Using Membrane Vesicles. The transport study was performed using a rapid filtration technique, as described previously (Kondo et al., 2004). In brief, 16 μl of transport medium (10 mM Tris, 250 mM sucrose, 10 mM $MgCl_2$, 10 mM creatine phosphate, 100 mg/ml creatine phosphokinase, and 5 mM ATP or AMP, pH 7.4, at 37°C) containing a tracer concentration (550 nM) of [^{3}H]E_1S was preincubated at 37°C and then rapidly mixed with 4 μl of membrane vesicle suspension containing 5 μg of membrane protein. The transport reaction was stopped by the addition of 1 ml of ice-cold buffer containing 250 mM sucrose, 0.1 M NaCl, and 10 mM Tris-HCl (pH 7.4 at 4°C). The stopped reaction mixture was passed through a 0.45-μm HAWP filter (Millipore Corporation, Billerica, MA) and then washed twice with 5 ml of stop solution. The radioactivity retained on the filter was measured using a liquid scintillation counter.

Cytotoxicity Assay. Cytotoxicity was assessed by the 3-(4,5-dimethylthiazol-2-yl)-2,5-diphenyltetrazolium bromide (MTT) method described previously (Lemos et al., 2008) with minor modifications. Cells were seeded at a density of 1.5×10^3 cells per 96-well plates (5.0×10^3 cells/cm^2) and incubated in antibiotic-free MEM medium supplemented with 10% FBS and 100 units/ml penicillin and streptomycin for 24 h. The cells were exposed to various concentrations of mitoxantrone dihydrochloride in the presence or absence of 5 μM FTC and cultured for additional 72 h. The drug-containing medium was discarded, 0.5 mg/ml MTT solution diluted by phenol red-free MEM medium (Invitrogen) was added, and the cells were incubated for an additional 4 h in the dark. The formazan crystals that had developed were dissolved in isopropyl alcohol supplemented with 0.4 N HCl at room temperature in the dark overnight. The absorbance at 540 nm was detected using a Multiskan JX microplate reader (Thermo Fisher Scientific, Waltham, MA).

Results

Effect of siRACK1 on the Cellular Localization of ABCG2. We first examined whether ABC transporters located on the bile canalicular membrane other than ABCB4 are regulated post-transcriptionally by RACK1. For this purpose, the cellular localization of exogenously expressed EGFP-tagged transporters in HeLa cells was examined. The expression of EGFP-ABCG2, which can be used to directly monitor ABCG2 expression and localization in living cells (Orbán et al., 2008), was affected by RACK1. As shown in the left panel of Fig. 1A, EGFP-fused ABCG2 localized predominantly on the plasma membrane of HeLa cells in the control conditions (Fig. 1A, left panel). In contrast, EGFP-ABCG2 localized intracellularly in almost all cells transfected with siRNA against RACK1, as observed for ABCB4 as shown in the right panel of Fig. 1A. In RACK1-suppressed HeLa cells, EGFP-ABCG2 localized intracellularly and colocalized partially with fluorescence-labeled ceramide, which is known to accumulate in the trans-Golgi region (Fig. 1B) (Lipsky and Pagano, 1985). In contrast, colocalization was not observed with

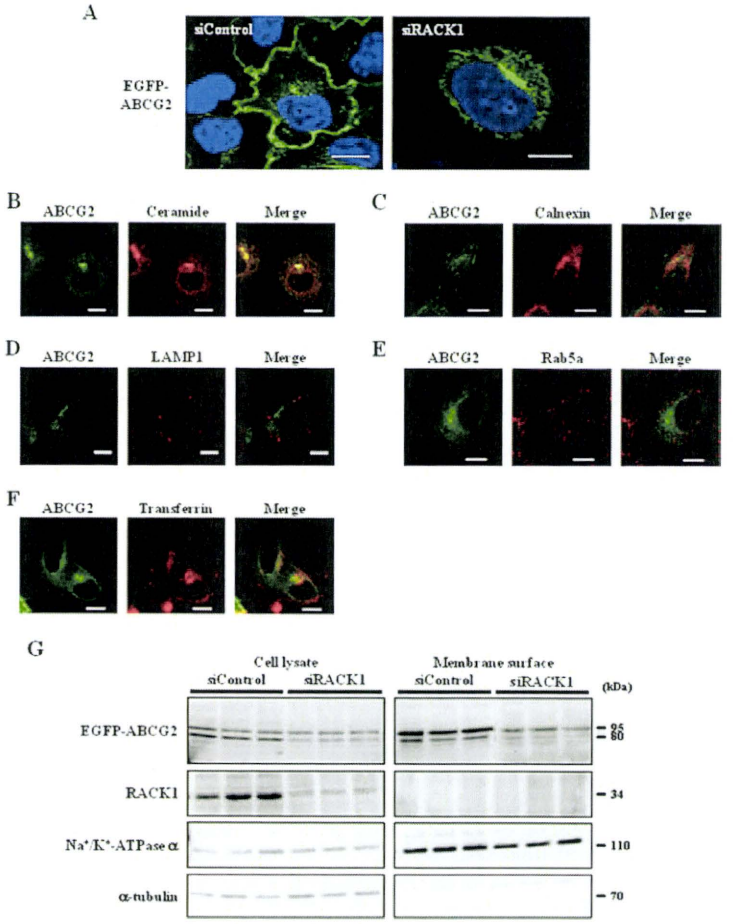

FIG. 1. Effect of RACK1 suppression on ABCG2 localization. A, cellular localization of EGFP-ABCG2 in HeLa cells. HeLa cells were transfected with EGFP-ABCG2 24 h after transfection with siRNAs and then cultured for an additional 48 h. Cells were fixed in methanol at −20°C, and the intracellular localization of EGFP-ABCG2 was observed using confocal microscopy. B to F, coimmunostaining of EGFP-ABCG2 with each organellar marker under the RACK1-knocked down conditions. Scale bar, 10 μm. G, membrane surface expression of EGFP-ABCG2 in HeLa cells. The amounts of EGFP-ABCG2, RACK1, Na^+/K^+-ATPase α, and α-tubulin expressed on the plasma membrane were determined using a biotinylation assay.

calnexin, LAMP1, Rab5a, or transferrin, organellar markers of the endoplasmic reticulum, lysosomes, early endosomes, and recycling endosomes, respectively (Fig. 1, C–F). These results suggest that RACK1 plays an important role in the post-trans-Golgi modification and localization of ABCG2 on the plasma membrane in HeLa cells. To confirm the effect of RACK1 suppression on the cell surface expression of EGFP-ABCG2, we performed a biotinylation assay and detected the amount of EGFP-ABCG2 on the plasma membrane (Fig. 1G). The efficacy of biotinylation with membrane proteins was validated by the expression levels of Na^+/K^+-ATPase α and α-tubulin, which are marker proteins of cell surface and cytoplasm, respectively. As indicated in the upper panel of Fig. 1G, cell surface expression of EGFP-ABCG2 was reduced by siRACK1 treatment, which may be consistent with the observation of EGFP-ABCG2 localization by confocal microscopy (Fig. 1A).

Because endogenous expression of ABCG2 was readily detected and relatively high compared with other cell lines tested (Supplemental Fig. A), we also examined the effect of RACK1 suppression on the cellular localization of endogenous ABCG2 in HeLa cells using two kinds of anti-ABCG2 antibodies, BXP-53 and 5D3 (Fig. 2). BXP-53 reacts with an internal epitope of ABCG2, whereas 5D3 reacts with an external epitope of ABCG2. As shown in Fig. 2, endogenous ABCG2 on the plasma membrane could be detected by 5D3 in HeLa cells without permeabilization but not by BXP-53. On the other hand, both BXP-53 and 5D3 could react with endogenous ABCG2 after the permeabilization treatment. Under control conditions, endogenous ABCG2 localized on the plasma membrane in almost all cells, whereas it localized in intracellular compartments in HeLa cells transfected with siRNA against RACK1 (Fig. 2). In addition, the amount of cell surface ABCG2, which was confirmed by 5D3 without permeabilization, was decreased by siRACK1 treatment. These results suggest that RACK1 regulates the intracellular localization of ABCG2 on the plasma membrane, and RACK1 suppression leads to the decrease of cell surface expression of endogenous ABCG2 in HeLa cells.

Positive Correlation between the Expression Levels of RACK1 and ABCG2. As shown in Fig. 2, the fluorescence intensity of endogenous ABCG2 decreased in RACK1-knocked down HeLa cells. This result suggests that RACK1 also regulates the protein expression of ABCG2. To examine this possibility, we constructed two kinds of HeLa cell lines whose RACK1 is knocked down, referred to as miRACK1*1 and miRACK*2, and HeLa cell lines stably overexpressing RACK1, referred to as RACK1*1 and RACK1*2. Compared with the miControl cells, endogenous RACK1 protein expression decreased to 54 and 56% in miRACK1*1 and miRACK1*2 cells, respectively, and endogenous ABCG2 protein expression also declined to approximately 50% (Fig. 3A). In contrast, in RACK1*1 and RACK1*2 cells, the increase in total expression of RACK1 protein, which is given as the sum of endogenous and exogenous myc-tagged RACK1 observed at 34 and 38 kDa, respectively, was associated with an increase in endogenous ABCG2 expression (Fig. 3A). These results indicate that the protein expression levels of ABCG2 and

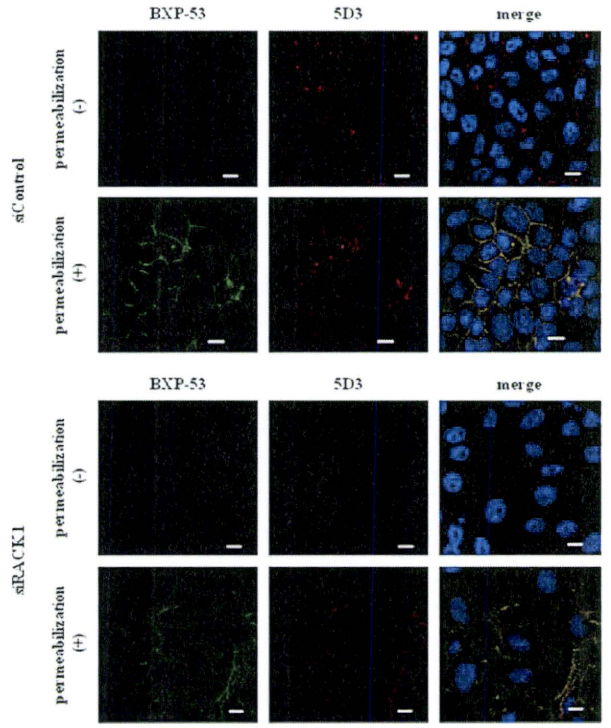

FIG. 2. Immunostaining of endogenous ABCG2 in HeLa cells. HeLa cells were fixed with paraformaldehyde with or without permeabilization treatment. Endogenous ABCG2 was visualized with anti-ABCG2 monoclonal antibody (BXP-53, green; 5D3, red) and the corresponding secondary antibody. The nucleus was stained with TO-PRO-3 iodide (blue). Scale bar, 10 μm.

RACK1 are positively related (Fig. 3B). ABCG2 mRNA expression was not affected by suppression or overexpression of RACK1 (Fig. 3C), suggesting that RACK1 regulates endogenous ABCG2 protein expression in a post-transcriptional manner.

We also used a biotinylation method to examine the cell surface expression level of endogenous ABCG2. As shown in Fig. 3D, compared with the expression level in the control cells, the cell surface expression of ABCG2 decreased in miRACK1 cells but increased in RACK1-overexpressing cells. These results are consistent with the results shown in Fig. 1.

Effect of RACK1 on the Stability of ABCG2 Protein. We have shown previously that RACK1 positively regulates the protein translation rate of ABCB4 but does not accelerate its degradation. Based on these findings, we examined whether the degradation of ABCG2 protein is affected by the suppression of endogenous RACK1. To examine this possibility, we tried to determine the half-lives of ABCG2 proteins in the presence of cycloheximide, a protein translation inhibitor. However, significant degradation of fully glycosylated ABCG2 (75 kDa) was not observed in either miControl or miRACK1 cells at 4 h, suggesting that the half-life of ABCG2 cannot be determined by this method (Fig. 4A). In addition, because of the very weak band density, we could not conclude whether the degradation rate of 60 kDa precursor protein, which may belong to immature forms of ABCG2, is different between miControl and miRACK1 cells. Furthermore, we also confirmed the effect of inhibitors (MG132, a proteasomal degradation inhibitor, and chloroquine, a lysosomal degradation inhibitor) for major protein degradation pathways. In many cases, protein degradation can be explained by these two degradation pathways. In the presence of MG132, the expression of immature ABCG2 (lower 60 kDa) was increased and showed almost the same level in miControl and miRACK1 cells, but this treatment did not affect the expression level of another immature (upper 60 kDa) and a mature fully glycosylated (75kDa) forms of ABCG2 (Fig. 4B). It was considered that the two immature ABCG2 bands located around lower and upper 60 kDa represented the nonglycosylated form and the core glycosylated form, respectively (Mohrmann et al., 2005). On the other hand, treatment with chloroquine did not affect the expression level of endogenous ABCG2 (Fig. 4C). We reasoned that, if RACK1 suppression enhances the degradation of ABCG2 via the proteasomal or lysosomal degradation pathway and it results in the suppression of endogenous ABCG2 expression, the protein expression level of endogenous ABCG2 in miRACK1 cells should be restored to almost the same level as that in miControl cells by MG132 or chloroquine treatments. However, this was not the case. These results suggest that the reduced expression of ABCG2 protein under the RACK1-knocked down conditions is not caused by the accelerated degradation of ABCG2 protein.

We next examined the involvement of RACK1 in the translational regulation of ABCG2 by monitoring ABCG2 protein synthesis using [^{35}S]methionine/cysteine. After initiation of metabolic labeling, two immature forms of ABCG2 appeared immediately, as observed previously (Imai et al., 2005). These nonglycosylated and core-glycosylated forms of ABCG2 shifted to the mature fully glycosylated form in both the miControl cells and miRACK1 cells in a time-dependent manner, although the proportion of mature form to immature form tend to be affected by RACK1 suppression (Fig. 4D, upper panel). In addition, the amount of newly synthesized ABCG2 in miRACK1 cells was not largely different from that in miControl cells. These results suggest that the reduction in the steady-state ABCG2 protein levels under RACK1-suppressed conditions (54–56% of miControl) (Fig. 3A) may not be absolutely ascribed to the suppressed protein synthesis.

[^{3}H]E_1S Transport Activity. To examine the functional activity of ABCG2 in RACK1-knocked down and -overexpressing cells, we prepared isolated membrane vesicles from these cells and assessed the uptake of [^{3}H]E_1S, a well known ABCG2 substrate. Reflecting the amount of ABCG2, the ATP-dependent transport activities differed between these cells (Fig. 5). [^{3}H]E_1S uptake was reduced to 63.1 $\pm$ 4.4 and 57.3 $\pm$ 8.1% of the control values in the isolated membrane vesicle prepared from miRACK1*1 and miRACK1*2 cells, respectively. In contrast, the transport activity in the isolated membrane vesicles from RACK1*1 and RACK1*2 cells increased to 134 $\pm$ 9 and 177 $\pm$ 3% of the control values, respectively. These results suggest that RACK1 regulates the cell surface expression of ABCG2 and consequently its functional activity.

ABCG2-Mediated Drug Resistance. We also used mitoxantrone to examine the effect of RACK1 expression on the anticancer drug resistance mediated by expression of ABCG2 (Scheffer et al., 2000). Although mitoxantrone is a dual substrate for ABCG2 and ABCB1, we assumed that we can examine the effect of RACK1 expression on the cellular function of ABCB2, because we have previously found that neither the expression level nor cellular localization of ABCB1 was affected by siRACK1 treatment in HeLa cells (Ikebuchi et al., 2009). HeLa cells whose RACK1 was knocked down stably and HeLa cells whose RACK1 was overexpressed stably were exposed to various concentrations of mitoxantrone and then subjected to the MTT assay (Fig. 6, A and B). We also constructed HeLa cells whose ABCG2 was knocked down stably, which are referred to as miABCG2 cells. The protein expression of endogenous ABCG2 in miABCG2 cells was almost the same as that in miRACK1 cells (data not shown). miRACK1*1, miRACK1*2, and miABCG2 cells showed higher

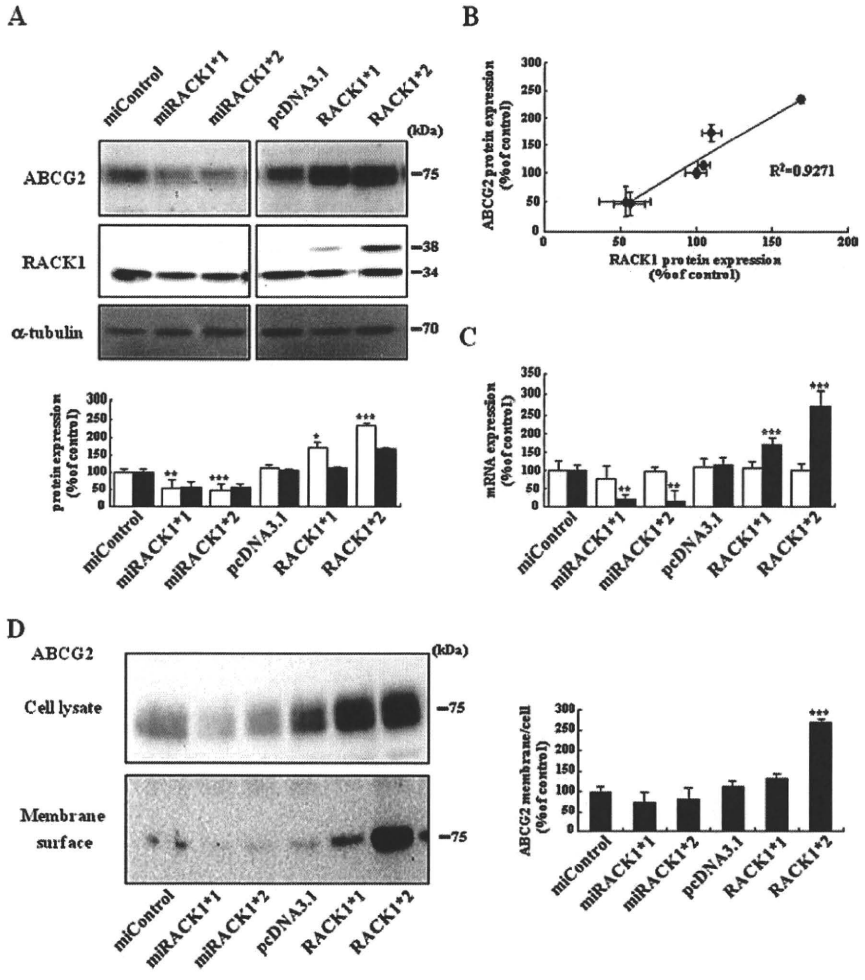

FIG. 3. Correlation between RACK1 and ABCG2 expression. A, protein expression levels of ABCG2 and RACK1. miControl, miRACK1*1, miRACK1*2, pcDNA3.1, RACK1*1, and RACK1*2 cells were prepared, and the expression levels of ABCG2 and endogenous and exogenous RACK1 were examined by Western blotting. The expression levels were normalized by those of miControl cells. □, protein expression of ABCG2; ■, protein expression of RACK1. The protein expression level of RACK1 was calculated as the sum of endogenous and exogenous RACK1. *, $p < 0.05$; **, $p < 0.01$; ***, $p < 0.001$, significantly different from the control cells by Student's t test. B, correlation of protein expression levels. Expression levels of ABCG2 (vertical axis) and RACK1, which is given as the sum of endogenous and exogenous myc-tagged RACK1 (horizontal axis), were plotted. Data were taken from Fig. 3A. Each value was normalized by that of miControl cells. C, mRNA levels of endogenous ABCG2 and RACK1. □, mRNA expression of ABCG2 (endogenous); ■, mRNA expression of RACK1. D, membrane surface expression of ABCG2. The amount of ABCG2 expressed on the plasma membrane was determined using a biotinylation assay. The total cell lysate and cell membrane surface expression of ABCG2 were normalized by those of miControl cells. ***, $p < 0.001$, significantly different from the control cells by Student's t test. The results are expressed as the mean ± S.D. of triplicate determinations.

sensitivity to mitoxantrone than did miControl cells (Fig. 6A). In contrast, RACK1*1 and RACK1*2 cells showed lower sensitivity to mitoxantrone and survived in the presence of a higher concentration of mitoxantrone (Fig. 6B).

To test the hypothesis that the difference in sensitivity to mitoxantrone between these cells is dependent on the expression level of ABCG2, we examined the effect of FTC, a selective inhibitor of ABCG2 (Fig. 6, C and D); in fact, 5 μM FTC inhibited the function of ABCG2 but not that of ABCB1 (Rabindran et al., 2000). If the difference in sensitivity to mitoxantrone is explained mainly by the different expression levels of ABCG2, the difference in the sensitivity should disappear with inhibition of ABCG2. miControl cells and miRACK1*2 cells showed almost the same sensitivity to mitoxantrone in the presence of FTC (Fig. 6C). In the same manner, the difference in cell viability with mitoxantrone between pcDNA3.1 control cells and RACK1*2 cells disappeared in the presence of FTC (Fig. 6D). In addition, the suppression or overexpression of RACK1 did not affect the endogenous expression of ABCB1 (data not shown), which is that of a drug transporter with a capacity for mitoxantrone secretion. These results suggest that RACK1 regulates both the protein expression and cellular localization of ABCG2, which are accompanied by changes in transport function as well as resistance to mitoxantrone.

Discussion

It is well established that ABCG2 excretes many kinds of anticancer drugs and plays an important role in multidrug resistance (Doyle et al., 1998; Haimeur et al., 2004). ABCG2 is up-regulated in several tumor tissues and affects the prognosis of patients with acute myeloid leukemia (Steinbach et al., 2002), although the precise regulatory mechanism is not understood fully. The estrogen receptor α regulates ABCG2 expression in a transcriptional manner (Imai et al., 2005), although there is little information on the post-transcriptional regulation of ABCG2.

In the present study, we examined whether RACK1 is involved in the regulation of the intracellular localization of ABCG2. We found that exogenous and endogenous ABCG2, which localized on the plasma membrane under basal conditions, localized intracellularly when the expression of RACK1 was suppressed by siRNA (Figs. 1A and 2). The effect of RACK1 suppression on ABCG2 localization was also confirmed by the biotinylation assay (Figs. 1G and 3D). ABCG2 is known to form a homodimer at the endoplasmic reticulum, and this dimer is translocated to the plasma membrane after glycosylation at the Golgi apparatus (Kage et al., 2002). It is possible that RACK1 mediates the dimerization or glycosylation of ABCG2 and consequently regulates the cell sur-

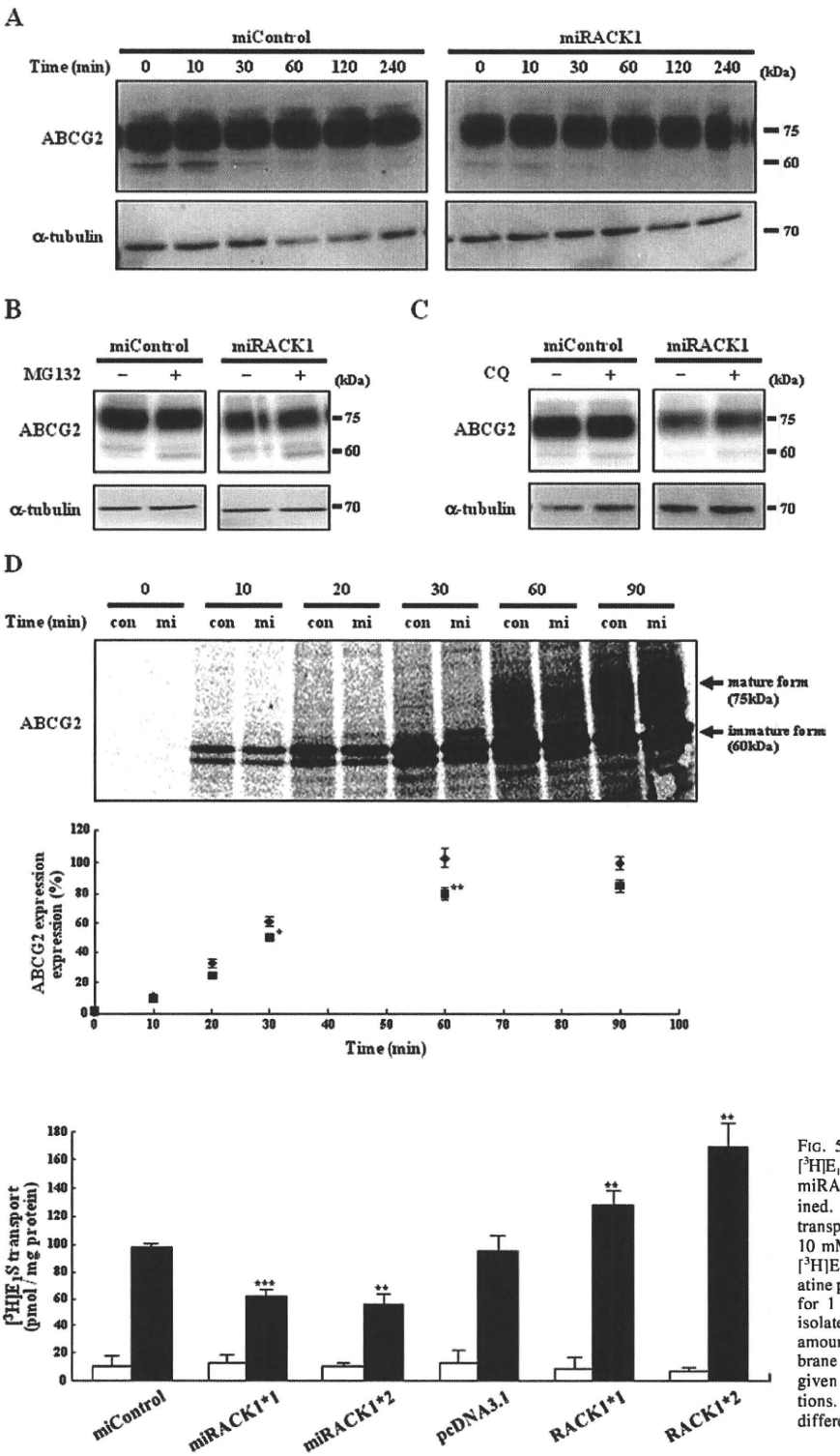

FIG. 4. Regulation of the expression of ABCG2 by RACK1. A, effect of RACK1 suppression on the degradation of ABCG2. Cycloheximide (100 μM) was added to the medium, and miControl cells and miRACK1*2 cells were collected at the times indicated. The protein levels of ABCG2 (top panels) and α-tubulin (bottom panels) were measured. B, effect of MG132 on the degradation of ABCG2. MG132 (5 μM) or vehicle (dimethyl sulfoxide) was added to the medium, and the cells were cultured for 24 h. Protein expression levels of ABCG2 and α-tubulin in each specimen were determined by Western blot analysis. C, effect of chloroquine on the degradation of ABCG2. Chloroquine (CQ) (250 μM) or vehicle (PBS) was added to the medium, and the cells were cultured for 6 h. The protein expression levels of ABCG2 and α-tubulin in each specimen were determined by Western blot analysis. D, effect of RACK1 suppression on protein synthesis of ABCG2. After preincubation in methionine/cysteine-free medium for 60 min, [^{35}S]-labeled methionine/cysteine was added for metabolic labeling. The cells were harvested at the times indicated to chase the expression level of ABCG2. The cells were lysed, and ABCG2 was immunoprecipitated using anti-ABCG2 rat monoclonal antibody (BXP-53). The proteins were separated by SDS-polyacrylamide gel electrophoresis and detected using a PhosphorImager. The band densities (mature form and immature form) were quantified and normalized by those in miControl cells at 90 min. ◆, protein expression of ABCG2 in miControl (con) cells; ■, protein expression of ABCG2 in miRACK1 (mi) cells. The results are given as the mean ± S.D. of triplicate determinations. *, $p < 0.05$; **, $p < 0.01$, significantly different from the control cells by Student's t test.

FIG. 5. [^{3}H]E_1S transport assay. The uptake of [^{3}H]E_1S by membrane vesicles isolated from miControl, miRACK1, pcDNA3.1, and RACK1 cells was examined. Membrane vesicles (5 μg) were incubated in transport buffer (10 mM Tris, 250 mM sucrose, and 10 mM $MgCl_2$, pH 7.4, at 37°C) containing 550 nM [^{3}H]E_1S, 10 mM creatine phosphate, 100 mg/ml creatine phosphokinase, and 5 mM AMP or ATP at 37°C for 1 min. □, amount of [^{3}H]E_1S taken up by the isolated membrane vesicles in the absence of ATP; ■, amount of [^{3}H]E_1S taken up by the isolated membrane vesicles in the presence of ATP. The results are given as the mean ± S.D. of triplicate determinations. **, $p < 0.01$; ***, $p < 0.001$, significantly different from the control cells by Student's t test.

face expression of ABCG2. Under the RACK1-knocked down conditions, ABCG2 colocalized partially with the marker for the Golgi apparatus but not with that of the endoplasmic reticulum (Fig. 1, B and C). This observation suggested that the reduced RACK1 expression does not affect homodimer formation at the endoplasmic reticulum. Regarding the latter possibility, the pro-

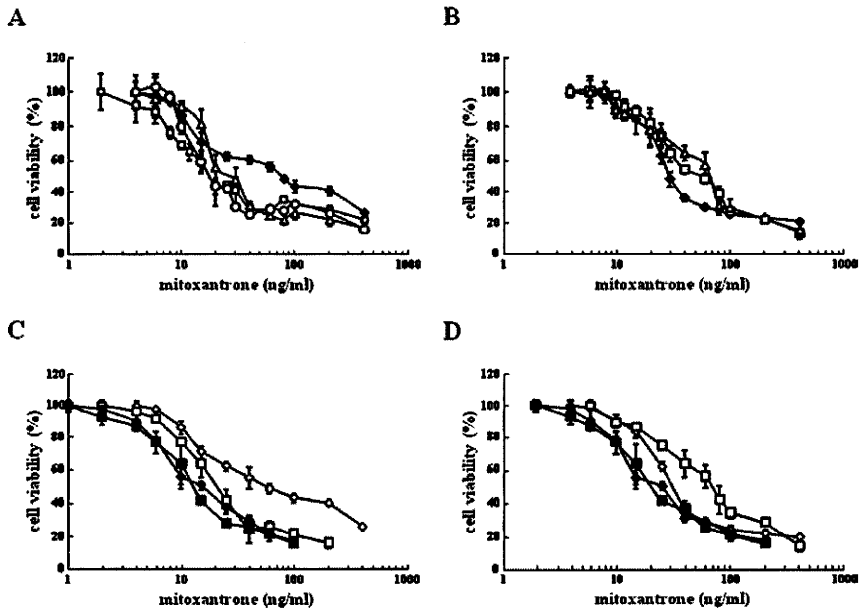

FIG. 6. Cell viability against mitoxantrone. A and B, cells were incubated with various concentrations of mitoxantrone for 72 h and then subjected to an MTT assay. A, results from miControl (◆), miRACK1*1 (□), miRACK*2 (△), and miABCG2 cells (○). B, results from pcDNA3.1 (◆), RACK1*1 (□), and RACK1*2 (△) cells. C and D, effect of FTC on mitoxantrone resistance. The MTT assay was performed to assess the viability of cells exposed to mitoxantrone in the presence or absence of 5 μM FTC. C, ◆, results from miControl cells in the presence of FTC; ◇, results from miControl cells in the absence of FTC; ■, results from miRACK1*2 cells in the presence of FTC; □, results from miRACK1*2 cells in the absence of FTC. D, ◆, results from pcDNA3.1 cells in the presence of FTC; ◇, results from pcDNA3.1 in the absence of FTC; ■, results from RACK1*2 cells in the presence of FTC; □, results from RACK1*2 cells in the absence of FTC.

portion of the mature to immature form of ABCG2, which indicates the extent of glycosylation of ABCG2 at the Golgi apparatus, tends to be affected by RACK1 suppression (Fig. 4D). From this result, it could be indicated that RACK1 regulates the glycosylation and maturation of ABCG2 at the Golgi. As an alternative, it is also possible that RACK1 is involved in the trafficking process of ABCG2 from the Golgi apparatus to the plasma membrane.

Together with the altered intracellular localization of ABCG2, we found a positive correlation between the protein expression levels of RACK1 and ABCG2 (Fig. 3, A and B). The lack of effect of RACK1 suppression or overexpression (Fig. 3C) on mRNA expression of endogenous ABCG2 suggests that RACK1 regulates ABCG2 protein expression in a post-transcriptional manner. The homodimer of ABCG2 is stabilized by intra- and intermolecular disulfide bonding and *N*-glycosylation at several amino acid residues (Wakabayashi-Nakao et al., 2009). A defect in these post-transcriptional modifications causes protein misfolding and subsequent degradation by the endoplasmic reticulum-associated degradation pathway, which is sensitive to MG132. Another study showed that the expression level of the ABCG2 C592G/C608G mutant, which lacks the intramolecular disulfide bond, was increased by MG132 treatment, whereas that of the wild type was not affected (Wakabayashi et al., 2007). In addition, it has been indicated that RACK1 is involved in the degradation pathway of several proteins by modifying the ubiquitination state (Ruan et al., 2009). RACK1 has been recently identified as a novel interacting partner of CLEC-2, a C-type lectin-like receptor, and this interaction regulates the stability of CLEC-2 through modifying its ubiquitin-proteasome degradation pathway. Therefore, it is possible that RACK1 suppression enhanced ABCG2 degradation and consequently caused the decrease in ABCG2 protein expression. However, we found that the inhibitor of proteasomal degradation, MG132, could not recover the expression level of the mature form of ABCG2 (Fig. 4B) under RACK1-knocked down conditions, although the immature, nonglycosylated form of ABCG2 was increased by this treatment in miControl and miRACK1 cells. These results suggest that the decreased expression of ABCG2 may not be caused by its accelerated degradation. Furthermore, it was indicated from the metabolic labeling experiment that reduced protein synthesis rate was not the sole mechanism of reduced protein expression of ABCG2 in miRACK1 cells. Although the precise mechanism for RACK1-dependent expression of ABCG2 remains to be clarified, the present results show the possibility that RACK1 may play multiple roles in the regulation of ABCG2 expression such as protein synthesis, maturation, and other unidentified process(es).

We also examined the function of ABCG2 under RACK1-suppressed conditions. Our results indicated that RACK1 regulates the cell surface expression of ABCG2 and consequently affects drug resistance. It has been well established that ABCG2 excretes a wide range of anticancer drugs and its expression is significantly associated with response and progression-free survival in patients with small cell lung cancer treated with platinum-based chemotherapy (Kim et al., 2009). In addition, it has been recently shown that elevated RACK1 expression is not only closely related to in vitro cell proliferation and invasion (Berns et al., 2000) but also linked to in vivo growth and metastasis of pulmonary adenocarcinomas and breast carcinomas (Cao et al., 2010; Nagashio et al., 2010). From these observations, it is possible that RACK1 can be attributed to tumor genesis and the multidrug resistance phenotype through the positive regulation of ABCG2. In contrast to ABCG2, ABCB1 and ABCC1 expression was not affected by RACK1 suppression (data not shown).

RACK1 is also involved in the acquisition of cellular drug resistance by affecting other mechanisms. For example, RACK1-overexpressing MCF-7 cells exhibit resistance to paclitaxel (Zhang et al., 2008). We confirmed these observations by Zhang et al. (2008) using established HeLa cell lines; in our experiments, RACK1*1 and RACK1*2 cells showed reduced sensitivity against paclitaxel, docetaxel, and vincristine, whereas miRACK1*1 and miRACK1*2 showed higher sensitivity to these anticancer drugs (data not shown). However, these phenomena may be independent of ABCG2 because the sensitivity to these drugs was not affected in miABCG2 cells (data not shown), and these drugs are poor substrates of ABCG2 (Litman et al., 2000). Although these drugs are substrates for ABCB1, the effect of RACK1 on drug resistance may not be mediated by ABCB1 because the localization and expression of ABCB1 were not affected